Preprint of Y. Zhang, S. A. Coronel, S. Lapointe, V. I. Thomas, R. M\'evel, A. Comandini, N. Chaumeix, and J. E. Shepherd. A comprehensive experimental and kinetic modeling study of flame speed and ignition delay time in n-hexane-based mixtures. Fuel 406 (2026) 136714. https://doi.org/10.1016/j.fuel.2025.136714

A comprehensive experimental and kinetic modeling study of flame speed and ignition delay time in n-hexane-based mixtures

Yakun Zhang[a], Stephanie A. Coronel[b], Simon Lapointe[b], Vaughan L. Thomas[c], Rémy Mével[d], Andrea Comandini[e], Nabiha Chaumeix[e], Joseph E. Shepherd[b]

[a]School of Vehicle and Mobility, Tsinghua University, Beijing, China
[b]Graduate Aerospace Laboratories, California Institute of Technology, Pasadena, California 91125, USA
[c]Department of Mechanical Engineering, Johns Hopkins University, Baltimore, Maryland 21218,USA
[d]School of Aeronautics and Astronautics, Zhejiang University, Hangzhou, China
[e]ICARE, CNRS-INSIS, 1C Avenue de la Recherche Scientifique, 45071 Orléans Cedex 2, France

*Corresponding author: mevel@zju.edu.cn

Abstract:
In the present study, laminar burning velocities of n-hexane/air mixture were investigated at equivalence ratios of 0.75-1.6, initial temperatures of 295-380 K and initial pressures of 40-100 kPa using two constant-volume chambers. Ignition delay times of stoichiometric n-hexane/O_2/N_2/Ar were measured in a shock tube at 1.2/2.0 MPa over 1150 to 1450 K. Based on existing literature on n-hexane oxidation and measurements from the current study, a database for n-hexane-based mixtures was established. The predictive performances of four chemical mechanisms were evaluated. The overall performance of Caltech mechanism is better for reproducing flame speed profiles, especially for rich n-hexane/air mixtures. LLNL mechanism predicts the ignition delay time well in the high-temperature range. Local and global sensitivity analyses at aircraft flight relevant conditions were performed. The laminar burning velocity is sensitive to R1: H+O_2=OH+O and R30: CO+OH=CO_2+H, and to the reactions involved in HCO formation/consumption. Ignition delay time is sensitive to reactions that contribute to OH radical formation before auto-ignition occurrence. Global sensitivity analyses were performed on laminar flame simulations and compared with the results of local sensitivity analyses. The global sensitivity analyses indicate limited/important reaction interactions under flame/ignition conditions.

Keyword: Laminar burning velocity; Spherically expanding flame; Ignition delay time; Shock tube; n-Hexane.

1 Introduction

Thermal ignition of reactive gas mixtures induced by hot surface or particle constitutes a hazard in industrial facilities and transportation systems. In aviation, the ignition source can be generated by lightning strike. Potential hazards include thermal ignition of fuel-air mixtures in a flammable fuel tank ullage or other unpressurized zone with the potential for flammable mixtures [1, 2]. Hot-surface ignition thresholds, or minimum surface temperature required for ignition, depend on a number of parameters such as the surface size, shape, orientation and influence of confinement on gas motion [3, 4, 5, 6, 7, 8]. During aircraft operation, the pressure within the fuel tank and other unpressurized regions of concern varies between 20 and 100 kPa. To assess the risk of potential ignition hazards and flammability in aircraft and other industrial settings, it is necessary to characterize combustion properties, such as laminar burning velocity (LBV) and ignition delay time (IDT) of fuel-air mixtures over a wide range of initial pressures and temperatures.

n-Hexane has been extensively used as a single-component of surrogate fuel for kerosene and diesel in our laboratory [6, 9, 10, 11]. This choice was motivated by the similar auto-ignition temperature of n-hexane and kerosene, i.e., around 500-505 K, whereas larger alkanes such as n-decane and n-dodecane demonstrate significantly lower values, i.e., 475-480 K, see [12]. In addition, n-hexane exhibits a relatively high vapor pressure which facilitates experimenting at ambient temperature. In contrast to n-heptane, which has been widely studied, n-hexane oxidation has received much less interest. The ignition delay times behind a shock wave were measured by Burcat et al. [13], Zhukov et al. [14], Javed et al. [15], Figueroa-Labastida et al. [16]. IDTs measured in rapid compression machine (RCM) and species profiles measured in jet-stirred reactor were also reported by Zhang et al. [17, 18] to explore the oxidation of hexane isomers and develop detailed chemical mechanisms. Houidi et al. [19] investigated the effect of temperature spatial and temporal variations in RCM on n-hexane auto-ignition. Mével et al. [20] employed a flow reactor along with gas chromatography (GC) analyses and laser-based diagnostics to measure the species profiles in the temperature range 600-1000 K. For laminar burning velocity measurement, experiments were implemented mostly at P≥100 kPa [21, 22, 23, 24, 25]. A limited number of studies have been found on the LBV measurement at initial condition with sub-atmospheric pressure.

Several mechanisms have been developed to describe the n-hexane combustion. Detailed mechanisms for n-hexane and hexane isomers were developed by Zhang et al. [17] and Zhang et al. [18], respectively referred to as Curran Mech and LLNL Mech in the present study. JetSurF mechanism [26], which is tailored for the combustion of jet-fuel surrogate, is commonly used for simulating n-hexane oxidation [27, 28, 29]. Besides, CaltechMech developed by Blanquart et al. [30] is also a relevant model due to its good ability at reproducing LBV for C_3-C_8 species. For completeness, we note that several other recent reaction mechanisms [31, 32] also include n-hexane chemical kinetics. To obtain a comprehensive validation of these mechanisms, it is required to establish an extensive database based on existing and

new experimental data for n-hexane combustion.

In the present study, laminar burning velocities were measured for n-hexane/air mixtures at atmospheric and sub-atmospheric pressures. Ignition delay times of stoichiometric n-hexane/O_2/N_2/Ar were measured in a shock tube at temperatures of 1150-1450 K and at pressures of 1.2/2 MPa. A comprehensive experimental database of ignition delay time and the laminar burning velocity for n-hexane-based mixtures (including the data from the present study) was established. This database was used to evaluate four existing hexane kinetic models (Curran Mech, LLNL Mech, JetSurF 2.0 and CaltechMech). Thermo-chemical analyses were implement to identify the key reactions that control the flame propagation and thermal ignition of n-hexane-based mixtures at aircraft operation related conditions. In particular, global sensitivity analyses were performed for the first time for such a large hydrocarbon molecule under laminar flame conditions.

2 Experimental database

Experimental laminar burning velocity and ignition delay time data for n-hexane-based mixtures were collected from published literature (LBV data: 111 points in 13 datasets from 6 publications, IDT data: 180 points in 20 datasets from 7 publications). Laminar burning velocities of n-hexane/air mixtures were measured using two approaches: spherically expanding flame (SEF) in constant volume/pressure chamber [27, 22, 24, 25] and counterflow or stagnation flame [21, 23]. Ignition delay time is usually measured by rapid compression machine (RCM) and shock tube (ST). A combination of RCM and ST data would benefit the exploration under temperature and pressure range of interest for engine combustion, especially for fuels showing negative temperature coefficient (NTC) behavior. For kinetic simulation of RCM, pressure or specific volume profiles of the corresponding non-reactive mixtures at each experimental condition are needed. However, these profiles are not always reported. For kinetic modeling of ST, constant volume behind the reflected shock wave is usually assumed. If the pressure rise caused by non-ideal effects cannot be ignored, a constant pressure rise dP_5/dt is used. We noticed that experiments using RCM were implemented under NTC region (T=700-900 K) which would not lead to successful thermal ignition for n-hexane/air mixtures. Considering the lack of pressure/volume traces from RCM experiments and thermodynamic conditions targeted for the current study, only IDT data measured in ST [17, 18, 13, 14, 15, 11, 16] were included in the database for the comparison of the models. Table 1 and Table 2 summarize the conditions employed to obtain the data included in the database. For detailed information on the experimental data, the reader should refer to the supplementary material. The measurements from the present study (LBV data: 37 points in 10 datasets, IDT data: 78 points in 4 datasets) were also included in the database for mechanism validation and comparison. It should be noted that, even though the number of data points is limited, discrepancies exist between measurements obtained in different studies. All data points were treated with equal weights in the present study. With the increase of data points obtained for various composi-

tions and at different conditions, the experimental database for n-hexane oxidation will become more complete in the future.

Table 1: The conditions of the experimental cases included in the LBV database for n-hexane/air mixtures.

Reference	P (kPa)	T (K)	Φ	Pts
Davis et al. 1998 [21]	101	298	0.75-1.7	13
Farrel et al. 2004 [22]	304	450	0.55-1.3	9
Ji et al. 2004 [23]	101	353	0.75-1.5	10
Kelley et al. 2011 [24]	101	353	0.75-1.7	19
	203	353	0.7-1.3	7
	507	353	0.7-1.1	5
	1013	353	0.7-0.9	3
Li et al. 2019 [25]	100	373	0.8-1.5	8
Zhang et al. 2019 [27]	60	353	0.8-1.6	9
	80	353	0.8-1.6	9
	100	353	0.8-1.6	9
	100	373	0.8-1.6	9
	100	393	0.8-1.6	9

3 Methodology

3.1 Experimental setups

Two constant-volume chambers were used to measure the laminar burning velocity: a cylindrical vessel at the California Institute of Technology (Caltech) [33] and a spherical reactor at ICARE-CNRS Orléans [34]. The volume of the cylindrical vessel is about 22 L. Parallel flanges are used to mount electrodes for the ignition system and optical windows with 117 mm diameter. The mixtures were ignited by an electric spark generated between two 0.4 mm in diameter tungsten electrodes separated by a distance of 2-4 mm. A high-speed camera (Phantom v711) was used to record the flame propagation observed using schlieren visualization and shadowgraphy at a rate of 10,000 frames per second with a resolution of 512×512 pixels. The experiments performed at Caltech were limited to temperatures up to 360 K. The experiments conducted at ICARE-CNRS were performed in a stainless steel spherical reactor with inner diameter of 475 mm. The mixtures were ignited by electric sparks with a nominal energy of 1.82 mJ. Schlieren visualization was used with a high-speed camera (Phantom V1610) at a rate of 25,000 frames per second with a resolution of 768×768 pixels. The experiments performed at ICARE were limited to temperatures above 360 K.

The high-temperature (1160-1450 K) ignition experiments at 1.2/2 MPa were carried out using a shock tube at ICARE-CNRS Orléans. A detailed description of the shock tube apparatus and diagnostics has been provided in [35]. Therefore,

Table 2: The conditions of the experimental cases included in the IDT database for n-hexane/O_2/diluent mixtures.

Reference	P (MPa)	T (K)	Φ	Dilution	Dilution ratio	Pts
Burcat et al.	0.36-0.43	1360-1520	1.0	Ar	89.50%	3
1996 [13]	0.38-0.40	1200-1430	0.5	Ar	79.80%	3
	0.34-0.38	1360-1760	2.0	Ar	94.25%	3
	0.36-0.37	1280-1570	0.5	Ar	90.00%	3
	0.30-0.32	1320-1460	1.0	Ar	79.00%	3
	0.35-0.36	1260-1460	2.0	Ar	88.50%	3
	0.76-0.84	1360-1480	1.0	Ar	94.75%	3
Zhukov et al.	1.15-1.40	1170-1380	0.5	N_2	78.13%	13
2004 [14]	5.57-6.69	1030-1350	0.5	N_2	78.13%	16
	20.87-24.72	820-1190	0.5	N_2	78.13%	11
Figueroa-Labastida	0.23-0.24	1080-1370	1.0	Ar	89.50%	4
et al. 2021 [16]	0.24-0.27	820-990	1.0	Ar	47.50%	3
He et al.	0.32-0.38	1300-1479	0.66	Ar	96.00%	9
2019 [11]	0.31-0.41	1300-1580	1.0	Ar	96.00%	11
	0.31-0.37	1340-1610	2.0	Ar	96.00%	18
Javed et al.	0.15	640-1260	1.1	Ar	51.00%	13
2017 [15]						
Zhang et al.	1.52	740-1360	1.0	N_2	77.29%	15
2015 [17]	1.52	750-1320	2.0	N_2	75.66%	17
	3.24	800-1350	1.0	N_2	77.29%	14
Zhang et al.	1.50	740-1360	1.0	N_2	77.29%	15
2019 [18]						

only a brief introduction is given here. The shock tube is made of stainless steel and has a 2-m driver section and a 5.15-m long driven section made. The inner diameters of the driver and driven sections are 114.3 and 52.5 mm, respectively. The incident shock wave velocity was measured using pressure transducers. Pressure and temperature conditions behind reflected shock waves were calculated based on shock velocities and initial conditions. The errors on calculated temperature and pressure are estimated to be 1% and 1.5%, respectively. For detection of the OH* radicals emissions, a HAMAMATSU R928 photomultiplier equipped with a narrow slit and a bandpass optical filter centered at 306 nm with full width at half maximum of 10 nm.

3.2 Analysis of experiments

3.2.1 Spherically expanding flame

To obtain the flame radius as a function of time, raw images were processed using algorithms implemented in Matlab, including flame edge detection and flame radius profile extraction. Details on these programs have been described in [36, 37]. The unstretched laminar flame speed with respect to the burnt side, S_b^0, was extracted following recommendations from recently published papers on optimization of laminar flame speed experiments [38, 39, 40, 41]. The steps to obtain flame properties (S_b^0 and Markstein length L_b) are described below.

To identify the effects of ignition energy and cellular flame formation and localize in which range they influence flame propagation, the extrapolation surfaces of flame properties using different flame radius ranges were plotted, as done in [40]. Four commonly-used models that describe the evolution for the flame front, linear stretch (LS) [42, 43], linear curvature (LC) [44], nonlinear model in expansion form (NQ) [45], nonlinear quasi-steady (NQ) [46], were all used for getting the extrapolation surfaces. If obvious surface folding or crest induced by non-ideal effects exists, the lower and upper bounds (R_{min} and R_{max}) would be set at the radii not affected by these perturbations. If the surface is wavy with small oscillations, all of the radius data would be used for fitting, since large size of radius data is beneficial for reducing the noise error [38, 39]. Numerical integration of these extrapolation equations was employed to avoid creating noise by numerically differentiating the experimental data. Example of extrapolation surfaces are shown in the supplementary material. The R_{min} and R_{max} obtained with the four extrapolation equations were pretty similar in general. After setting flame radius range, we followed the recommendations from [38]: selection of the extrapolation equation should be based on the capabilities of extrapolation equations to reproduce flame propagation profile. The profiles of flame radius with time ($R_f(t)$) integrated using four extraction models were compared with experimental $R_f(t)$. Goodness of fit (R^2) was calculated for checking the performance of extrapolation equations. Consistent with the numerical results from [38], with Markstein length gradually deviating from zero, the experimental S_b^0 and L_b derived by different extraction models show larger deviation, especially for those derived using LS and NQ. Differences are smaller for parameters extrapolated by LC and NE models. Examples of fitted results are shown in Figure 1. From Figure 1,

we can see that R^2 is generally very large (>0.99) when there is enough radius data points. Two circumstances were observed: i) the calculated R^2 using the different extrapolation models are very close to each other (the left figure in Figure 1); ii) the R^2 of LS model is lower than that of nonlinear models (the right figures in Figure 1). Then, for circumstance i), the average values of S_b^0 and L_b derived by four models were considered as the final properties. For circumstance ii), the ultimate S_b^0 and L_b are determined as the average values obtained with the three nonlinear models. See supplementary material for examples of extrapolation curves. The uncertainty of the flame properties is determined to be twice the maximum absolute difference between the extrapolated values by 4 models (for circumstance i) or 3 nonlinear models (for circumstance ii) and their average value. The extrapolation error induced by different models and random noises, such as flame edge detection, and the errors on initial condition and mixture preparation were considered to obtain such uncertainty. Then, the unstretched laminar flame speed was calculated as $S_u^0 = (\rho_b/\rho_u)S_b^0$, where ρ_b and ρ_u are the densities of the burnt and fresh mixture, respectively.

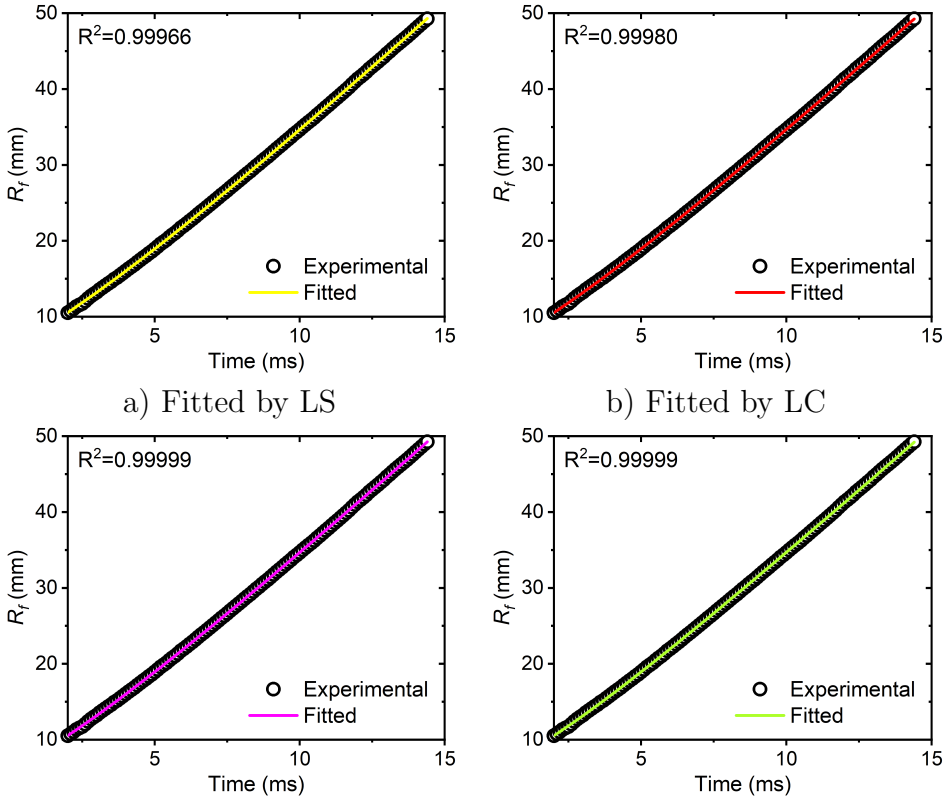

a) Fitted by LS b) Fitted by LC

a) Fitted by NE b) Fitted by NQ

Figure 1: Examples of fitted flame radii with time using four extrapolation models. Conditions: n-hexane/air mixtures, P=50.0 kPa, T=295 K, Φ=1.1.

3.2.2 Shock tube

For the determination of ignition delay time, two definitions were used: (i) the time to maximum slope of signal extrapolated to the baseline for pressure profile, (ii) the time to the slope of half OH* emission maximum extrapolated to the emission baseline. Typical pressure and OH* profiles are provided in Figure 2. The uncertainty on the characteristic reaction times is estimated to be 10%. Such uncertainty is mainly induced by the shape of OH* emission profile and the identification of the auto-ignition onset. Note that, under some of the conditions we employed, pressure rise due to non-ideal effects in shock tube cannot be ignored. The rate of pressure increase behind the reflected shock wave and the ignition delay time data are reported in the supplementary material.

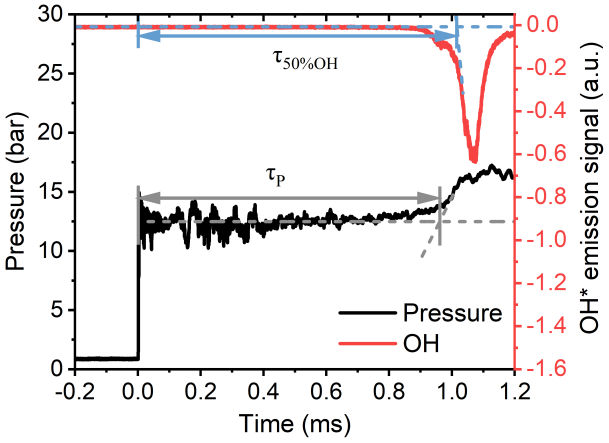

Figure 2: Typical pressure and OH* profiles obtained during ignition of a stoichiometric n-hexane/O_2/N_2/Ar mixture behind a reflected shock.

3.3 Analyses of reaction models

3.3.1 Error function

For evaluating the capabilities of the chemical mechanisms to reproduce fundamental flame properties, the method of Olm et al. [47] was employed. The error score of the i^{th} experimental data point is calculated as

$$E_i = \left(\frac{Y_i^{sim} - Y_i^{exp}}{\sigma\left(Y_i^{exp}\right)} \right)^2, \tag{1}$$

where Y_i^{sim} and Y_i^{exp} are respectively the simulated and experimental parameters, $\sigma\left(Y_i^{exp}\right)$ is the experimental uncertainty factor. Uncertainty of LBV data is characterized by absolute error. In this case, Y is the unstretched laminar flame speed S_u^0, $\sigma\left(Y_i^{exp}\right)$ is the error of the reported LBV ($\delta_{S_u^0}$). However, the error range is not given in some literature. Uncertainties of all the S_u^0 measurement methods have been discussed by Egolfopoulos et al. [48]. The values ±5% and ±3% are the recommended uncertainty range for stagnation flame and SEF. Possible sources of

uncertainty for S_u^0 measurement using SEF were reviewed in [41, 49]. It turns out that determination of the uncertainty factor is related to several aspects, such as mixture preparation, ignition energy, stretch extrapolation. Given the complexity of determining this uncertainty factor, the middle value (2 cm/s) of reported errors from published literature was used as $\delta_{S_u^0}$ when experimental uncertainty factor is not provided. Maximum and minimum $\delta_{S_u^0}$ are 3.25 cm/s (Φ=1.5, from [25]) and 0.70 cm/s (Φ=1.1, from [23]).

Different from LBV, relative error is usually used to describe the uncertainty range for IDT data. Therefore, Y would be $\ln\tau$, where τ is the ignition delay time. $\sigma\left(Y_i^{exp}\right)$ corresponds to $\ln(1+\delta_\tau)$ where δ_τ is the uncertainty on the experimental ignition time. The value δ_τ=20% is specified when the error range is not given in the literature, since 20% is a typical uncertainty factor for ST-measured IDT[50, 11, 51, 52, 53]. For a dataset, the error score is calculated as

$$E = \frac{1}{N}\sum_{i=1}^{N} E_i. \tag{2}$$

Error function value would be close to unity if the chemical mechanism could reproduce the combustion properties well.

The performances of four mechanisms (CaltechMech, 193 species and 1168 reactions, JetSurF 2.0, 348 species and 2163 reactions, Curran Mech, 1118 species and 4808 reactions, LLNL Mech, 1709 species and 6854 reactions) in predicting fundamental combustion properties for n-hexane-based mixtures were evaluated based on LBV and IDT data from published literature and the present study. Error scores of all the datasets have been reported in the supplementary material.

3.3.2 Kinetic analyses

Numerical simulations for flame properties and kinetic analyses were performed using Cantera [54]. The flame speed simulations for global sensitivity analyses were performed using the LLNL code [55]. Shock tube experiments were simulated using the adiabatic constant volume reactor model. LBV data were obtained using the freely propagating flame code with multi-component transport properties. Soret effect was also considered. Various kinetic analyses, including analyses on heat release rate (HRR), rate of production (ROP), and local sensitivity analyses (LSA), were performed to identify key reactions for n-hexane oxidation under specific thermodynamic conditions. Local sensitivity factor for reaction i was calculated as $C_S(i) = (k_i/y)(\partial y/\partial k_i)$, where k and y are respectively the i^{th} reaction rate constant and the target parameter. For laminar flame experiments, y is the laminar flame speed. For shock tube experiments, two targets are set: one is ignition delay time (defined as the time corresponding to the maximum rate of change for pressure profile), the other one is temperature. Through integrating $C_S(i)$ over the test time, overall sensitivity coefficients were obtained.

Local sensitivity analysis is a useful analysis tool for models when the uncertainty range of input parameter is small [56]. However, for investigations on the

nonlinear models with highly-uncertain input parameters and the joint effects of multi-variables on the outputs [57], global sensitivity analysis (GSA) should be employed to analyze the complex reaction systems. It is noted that GSA can also be employed for model optimization and reduction. In the present study, in addition to local sensitivity analyses, we also conducted global sensitivity analyses for laminar flame speed and ignition delay time. The definition of IDT is the same as that of local sensitivity analyses. There are many methods developed for global sensitivity analysis. In the present study, the Sobol sensitivity technique was employed. This technique has been described in detail by Lin et al. [58]. The procedures for performing GSA is briefly described as follows. Sobol sensitivity analysis is a technique based on variance decomposition. The variance of the output for the complex model can be decomposed into fractions which can be attributed to input parameters. The model can be described as a function, $Y = f(x)$, where x is a vector of n model inputs with uncertainty $(x_1, x_2, ..., x_n)$ defined in the unit hypercube, i.e., $x_i \in [0, 1]$ for i=1, 2, ..., n. The function $f(x)$ can be decomposed as [59]:

$$Y = f_0 + \sum_{i=1}^{n} f_i(x_i) + \sum_{1 \le i < j \le n} f_{ij}(x_i, x_j) + ... + f_{1,2,...,n}(x_1, x_2, ..., x_n). \tag{3}$$

For independent inputs, a unique decomposition in orthogonal terms exists. The following condition should be satisfied for the analysis of the variance representation of $f(x)$:

$$\int_0^1 f_{i_1,...,i_s}(x_{i_1}, ..., x_{i_s}) dx_k = 0, \tag{4}$$

for $k = i_1, ..., i_s$, $1 \le i_1 < ... < i_s \le n$. Through integrating both sides of Equation 3, the decomposition of variance can be expressed as,

$$Var(Y) = \sum_{i=1}^{n} V_i + \sum_{i<j} V_{ij} + \sum_{i<j<l} V_{ijl} + ... + V_{1,2,...,n}, \tag{5}$$

where V_i is the variance of $f_i(x_i)$, V_{ij} is the variance of $f_{ij}(x_i, x_j)$ and so on. For chemical kinetic system, the first-order sensitivity index for the ith reaction can be obtained as follow:

$$S_{R_i} = \frac{V_{R_i}}{Var(Y)}, \tag{6}$$

where V_{R_i} is the variance caused by reaction i, $Var(Y)$ is the variance induced by all reactions (including the mixed interactions of multiple reactions). The total sensitivity index for the ith reaction can be calculated as:

$$S_{TR_i} = 1 - S_{\sim R_i} = 1 - \frac{V_{\sim R_i}}{Var(Y)}, \tag{7}$$

where $V_{\sim R_i}$ is the variance which is not caused by reaction i, $S_{\sim R_i}$ is a sensitivity index for all reactions but the ith reaction. Difference between S_{TR_i} and S_{R_i} is the sum of higher-order sensitivity indices which represent the joint impacts of two or more reactions on the model output. The sampling technique of Sobol sequences

was employed to generate a set of possible values for inputs based on the uncertainty factor (UF) for each reaction. Uncertainty factor of rate constant can be defined as,

$$UF = \frac{k_0}{k_{min}} = \frac{k_{max}}{k_0}, \tag{8}$$

where k_0, k_{min}, and k_{max} represent the mean, minimum, and maximum rate coefficient for one reaction. UF may be provided in kinetic model compilation. GSA with different sample sizes should be implemented in order to obtain the accurate and converged sensitivity index. To obtain first-order or total sensitivity index for a specified reaction under a specified sample size, the number of simulation cases needed equals this specified sample size. Therefore, the number of simulation cases needed for calculating first-order and total sensitivity indices for all reactions in the mechanism equals twice the reaction numbers times the sample size.

3.3.3 Investigated conditions

For detailed kinetic analyses, stoichiometric (Φ=1.0) n-hexane/air mixture and thermodynamic conditions related to thermal ignition in a fuel tank for aircraft were selected for further kinetic investigation. The main steps for a potential hot-surface ignition are illustrated in Figure 3. After lightning strike on composite aircraft structures, high temperature particles and gas jets may be ejected from the strike region. Unnotched and filled-hole Carbon Fiber Reinforced Polymers (CFRP) specimens were tested by Feraboli and Miller at different current levels to simulate lightning strike damage [60]. Potential sources of ignition from lightning strike on a fastener in a composite panel are shown in Figure 3, these include jets of hot gases, and particulates. The potential for ignition by hot gas jets in hexane-air mixtures was examined by Qi and Shepherd [61]. The potential for ignition by hot particles (spheres) in hexane-air mixtures was investigated experimentally and numerically by Coronel et al. [9]. Ignition occurs within the thermal boundary layer, slightly away from the surface of the sphere, where chemical energy release exceeds heat losses to the wall. In the region where the gas temperature is high enough to activate chemical reactions, an ignition kernel is formed and a flame propagates away from the ignition kernel. The high computational cost of the two-dimensional simulation performed by Coronel et al. makes it impractical to perform sensitivity analysis. Planes are usually struck by lightning at an altitude of 5,000 to 15,000 feet [62]. We selected the thermodynamic conditions as P_{in}=70 kPa and T_{in}=280 K, that corresponds to the conditions for an intermediate altitude (10,000 feet). Such conditions were used as the initial thermodynamic state for reaction rate sensitivity studies described in the next section. Temperature conditions for auto-ignition analyses were selected based on the ignition thresholds measured experimentally. For sphere temperature of 1224 K, probability of successful ignition was found to be 90% at initial temperature and pressure of 298 K and 100 kPa for lean n-hexane/air mixture (Φ=0.9) [9]. Boeck et al. [6] studied the ignition thresholds from heated circular cylinder. At standard conditions, stoichiometric n-hexane/air mixture ignited at about 1180 K and about 1270 K for the horizontally and vertically oriented cylinder, respectively. The effects of surface size were examined by Jones and Shepherd [7], Martin

[63] and the effects of ambient pressure by Martin and Shepherd [64]. Based on the above discussions, initial conditions of 70 kPa and 1250 K were selected as realistic for studying chemical kinetic relevant to hot-surface-induced thermal ignition.

For completeness, we note that determining appropriate surrogates for complex fuels such as kerosene is a very difficult task. First, a kerosene corresponds to a mixture of hundreds of hydrocarbons. The composition of kerosene is highly variable, depending on various factors, such as the origin of the crude oil employed to produce it, the specificity of the refining process, and the period of the year [65]. Another aspect to consider when studying safety in aircraft corresponds to the local thermodynamic state, which would greatly influence the local gas phase composition, due to the different vapor pressures of the kerosene's constituents. The mass loading, i.e., the amount of liquid fuel in the fuel tank, also influences the vapor composition. It should also be noted that for laboratory experiments, the utilization of complex fuels or multi-component surrogates that include heavy hydrocarbons is complicated. It is required to significantly heat the experimental facility to fully vaporize the fuel blend. Such a process may lead to partial oxidation of the fuel-air mixture before the experiments could be performed, see [66]. Finally, in a fuel tank, it is expected that gradients of concentration are present. Therefore, it is difficult to define the most relevant equivalence ratio. While it would be relevant to study a range of equivalence ratios, it would be too expensive to perform global sensitivity analysis for more than couple cases. All these aspects have motivated our choice to consider a stoichiometric n-hexane-air mixture since it can be considered as a reference mixture composition.

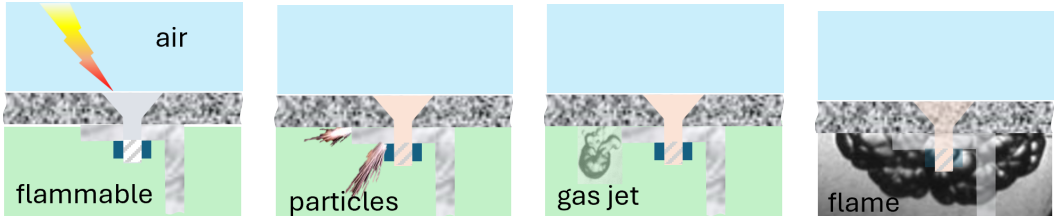

Figure 3: Schematic of possible sequence of events in ignition occurrence in an aircraft fuel tank following a lightning strike.

4 Results and discussion

4.1 Experimental results and models performance

4.1.1 Laminar burning velocity results

Experimental laminar flame speeds at atmospheric pressure along with the predictions of the four chemical models are shown in Figure 4. At ambient temperature, measurements made for lean and stoichiometric mixtures are relatively similar in the present study and in the study of Davis and Law [21]. For a rich mixture,

larger discrepancies exist between the two studies. It is noted that such discrepancies are often observed for rich mixtures between flame speed data obtained using SEF, as used in the present study, and using counterflow burner, as done in Davis and Law. A similar trend is observed in Figure 4 b) between the data of Kelley et al. [24], obtained using SEF, and the data of Ji et al. [23], obtained using a counterflow burner. We observe that S_u^0 calculated by CaltechMech is larger than that calculated by the three other mechanisms. Flame speeds predicted by JetSurF 2.0, Curran Mech and LLNL Mech are closer to the experimental measurements for Φ <1.0. However, for Φ ≥1.0, CaltechMech performs significantly better. At initial temperature of 353 K, large differences are observed between the three experimental study from the literature, especially for measurements from [27]. Curran Mech and LLNL Mech reproduce the experimental laminar burning velocities for rich mixtures from [23] well. Concerning the flame speed results for lean mixtures, larger discrepancies between the experimental data and the models prediction are observed.

The evolution of the laminar burning speed as a function of equivalence ratio was studied at initial pressure of 50 kPa, see Figure 5. Similar to the results at 100 kPa, flame speeds calculated by JetSurF 2.0, Curran Mech and LLNL Mech are lower that those calculated by CaltechMech. LBV cannot be captured well by all the models for the leanest n-hexane/air mixtures. Although CaltechMech over-estimates S_u^0, the deviation is lower than that of the other three mechanisms. Comparing the deviations between experimental values and the predictions of the four chemical models, CaltechMech shows better performance at low initial pressure and temperature. Therefore, it is used for the kinetic analyses for flame propagation presented in a later section.

The effects of initial pressure and temperature were also studied. Pressure effect for lean n-hexane/air mixture at initial temperature around 353 K is shown in Figure 6. We anticipate that laminar flame speed decreases with the increase of initial pressure. Based on the numerical simulation, the descending rate is faster at initial pressure lower than 200 kPa. Temperature effect at three equivalence ratios 0.9/1.1/1.4 and initial pressure of 50 kPa is shown in Figure 7. It can be expected that laminar burning velocity increases with increasing initial temperature. For Φ=0.9, laminar burning velocity is over-predicted by all four mechanism. For stoichiometric mixture, Curran Mech and LLNL Mech show better capabilities at predicting the LBV than JetSurF 2.0 and CaltechMech. For Φ=1.4, laminar burning velocity is over-estimated by CaltechMech and under-estimated by JetSurF 2.0, Curran Mech and LLNL Mech. The lowest error in the predictions of the LBV is achieved by CaltechMech, both considering the data obtained during the present study and the complete LBV database. Therefore, CaltechMech was selected to perform the sensitivity analyses presented in section 4.2.

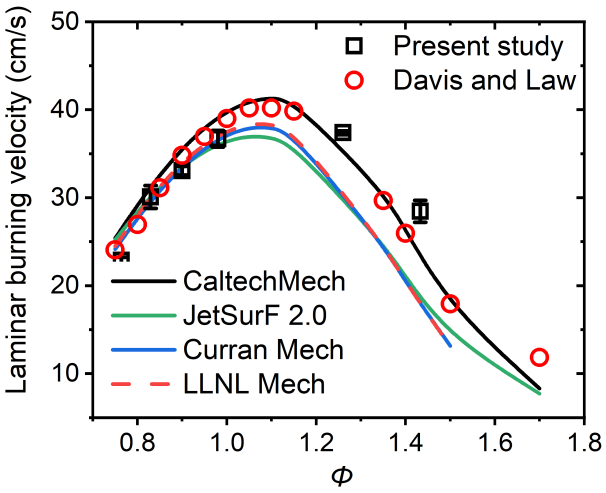

a) Initial temperature is around 298 K

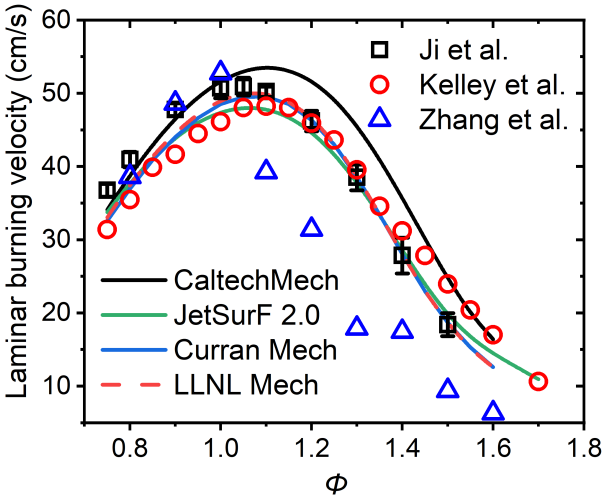

b) Initial temperature is around 353 K

Figure 4: Laminar burning velocity as a function of equivalence ratio for n-hexane/air mixtures at initial pressure of 100 kPa.

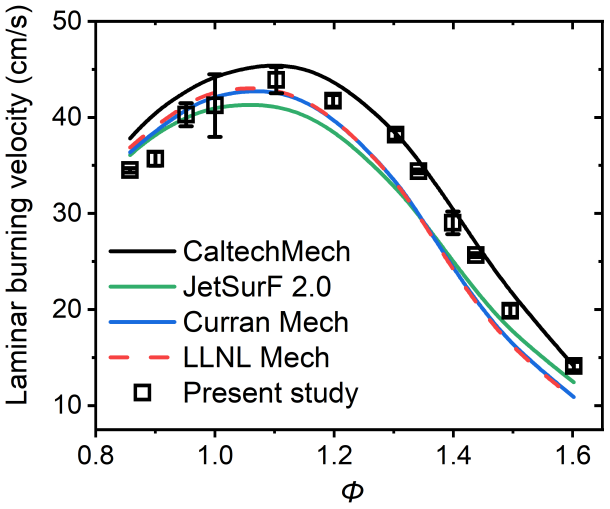

Figure 5: Laminar burning velocity as a function of equivalence ratio for n-hexane/air mixtures at initial temperature and pressure of 295 K and 50 kPa, respectively.

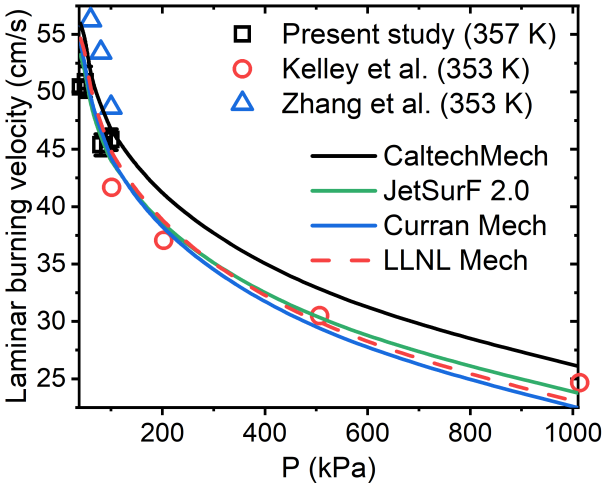

Figure 6: Laminar burning velocity as a function of initial pressure for n-hexane/air mixtures (Φ=0.9).

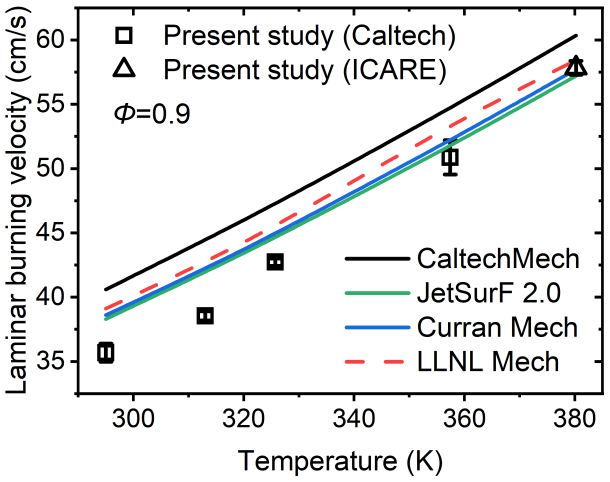

a) Lean mixture

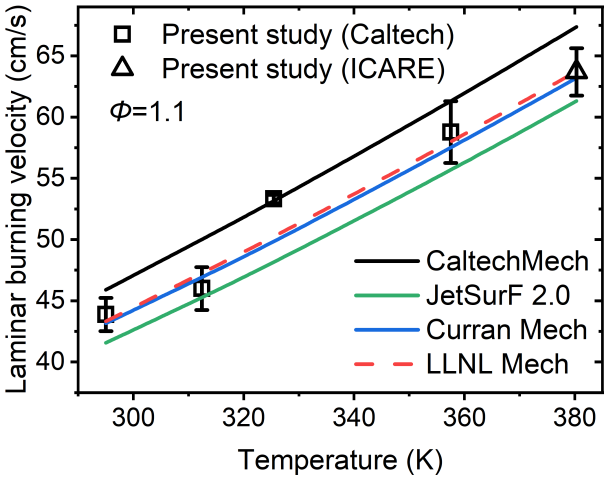

b) Stoichiometric mixture

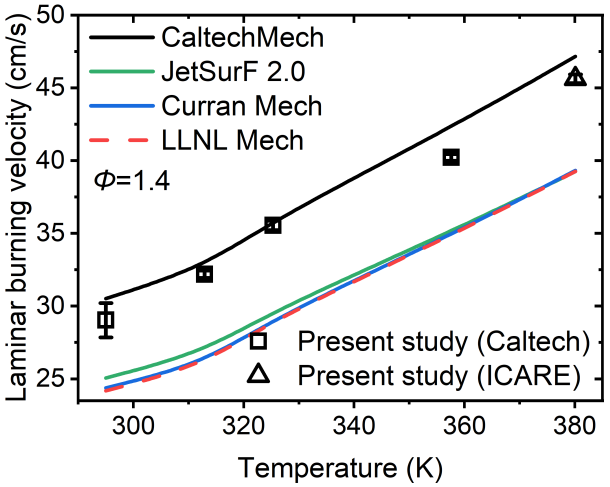

c) Rich mixture

Figure 7: Laminar burning velocity of n-hexane-air mixtures as a function of initial temperature at an initial pressure of 50 kPa and Φ=0.9/1.1/1.4.

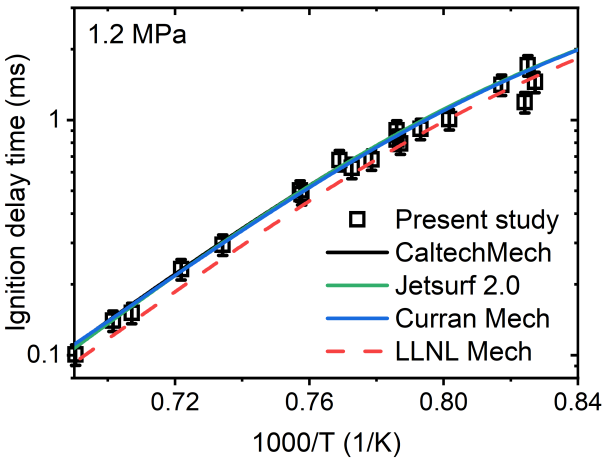

a) Pressure is around 1.2 MPa

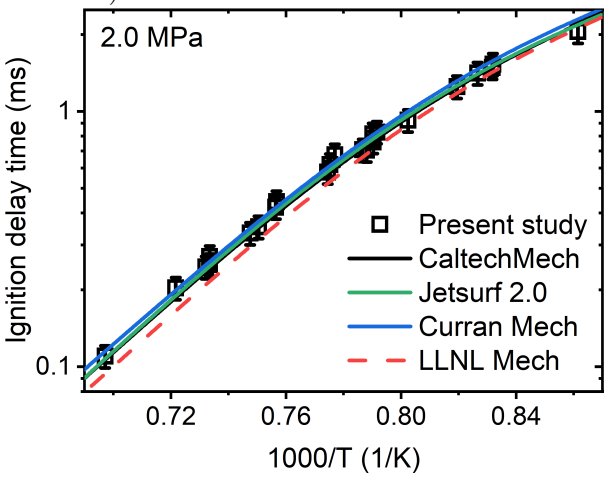

b) Pressure is around 2.0 MPa

Figure 8: Ignition delay time based on OH* as a function of temperature for n-hexane/O_2/N_2/Ar mixtures.

4.1.2 Ignition delay-time results

Experimental and numerical ignition delay times based on OH* for n-hexane/O_2/N_2/Ar mixtures at pressures of 1.2 and 2 MPa are shown in Figure 8. NTC behavior is not observed in Figure 8 due to the high-temperature range used for the measurements. It should be noted that dP_5/dt is different for each experiment. Different pressure rise behind the reflected shock wave and slightly different reflected shock pressures are the main causes for the deviation between data points with similar or close temperature conditions. In all cases, the same definition was employed for the ignition delay-time obtained experimentally and numerically. The predictions of LLNL Mech are always lower than the other three mechanisms. Considering the experiments of the present study, the four reaction mechanisms provide predictions of relatively similar accuracy, i.e., within 50% in most cases. Considering all the shock tube data, the discrepancies of Curran Mech and LLNL Mech are lower, i.e.,

below a factor of 2, than that of CaltechMech (factor of 2.2) and JetSurf (factor above 4.3). The LLNL Mech was used in the further thermo-chemical analyses under hot-surface-induced thermal ignition.

4.2 Thermo-chemical analyses

Due to the large number of kinetic simulation cases needed for global sensitivity analyses, the computational cost caused by using detailed mechanism is a challenge. Therefore, two mechanisms (CaltechMech for flame propagation analyses and LLNL Mech for ignition analyses) for global sensitivity analyses were reduced. For CaltechMech, C_7-C_{12} sub-mechanisms were removed to form a C_1-C_6 kinetic model (containing 85 species and 596 reactions). LLNL Mech was reduced using DRGEP (directed relation graph with error propagation) method. The reduced LLNL Mech contains 163 species and 1206 reactions. Comparisons for combustion properties, thermodynamic parameter and species profiles between the initial mechanisms and reduced mechanisms are presented in the supplementary material. It turns out that the flame propagation processes predicted by initial CaltechMech and reduced CaltechMech are similar under various initial conditions. The relative error between IDTs predicted by detailed LLNL Mech and reduced LLNL Mech is lower than 5% at temperature of 1200 to 1300 K and pressure of 69 to 71 kPa. After reducing the mechanisms, an uncertainty factor must be defined for each reaction in the reduced mechanisms in order to carry out the global sensitivity analyses. We assigned a factor of 2 for all reactions which is the conventional choice from previous studies examining uncertainty of kinetic parameters [67, 68, 69]. Reduced CaltechMech and LLNL Mech were employed to implement all the kinetic analyses. Different sample sizes were tested to get the converged sensitivity index for GSA, see the supplementary material for detail. For the reduced CaltechMech under target conditions, calculated sensitivity indices are similar between sample sizes of 1024 and 2048. For reduced LLNL Mech, global sensitivity indices calculated with sample sizes of 2048 and 4096 are close. Therefore, the results that we present in the later subsection are based on sample sizes equal to 2048 and 4096 for kinetic GSA of flame propagation and auto-ignition, respectively. The presented results were obtained based on 2,441,216 flame speed simulations and 9,879,552 auto-ignition simulations.

4.2.1 Analyses for flame propagation

LSA and GSA are two complementary but different analyses. LSA basically consists in determining the impact of a single reaction by evaluating the local rate of change of a model output as a specific input parameter is perturbed. As detailed in section 3.3, GSA is a much more complex analysis which takes into account the input uncertain and provides information on the impact of interactions of input parameters on the model output. Therefore, it could be expected that the LSA and GSA results are not fully similar, although qualitatively consistent results could be obtained under certain conditions as in Zador et al. study [68]. In Fig. 9 and 10, it is interesting to note that common reactions with dominant local and global sensitivities correspond to R1: $H+O_2=OH+O$ and R30: $CO+OH=CO_2+H$. These two reactions appear as sensitive in most combustion relevant conditions, owing to their prominent impact on the

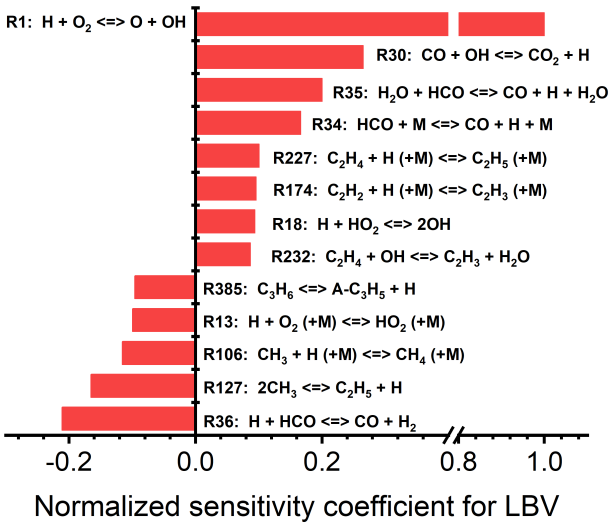

Figure 9: Normalized local sensitivity coefficient on the laminar burning velocity for stoichiometric n-hexane/air mixture under initial conditions of T_0=280 K, P=70 kPa.

chain-branching process, and heat release rate, respectively. This result is consistent with the results of Zador et al. [68] who implemented both LSA and GSA for laminar flame speed of methane-air mixtures. Reactions involving HCO, i.e., its decomposition to CO+H, and its reactions with H_2O and H, also demonstrate both significant local and global sensitivity coefficients. On the other hand, reactions of HCO with OH, including R38: HCO+OH=CO+H_2O and R75: O_2+T-CH_2=HCO+OH, show negligible sensitivity coefficients. The reactions of the low-temperature sequence R13: H+O_2+M=HO_2+M followed by R18: H+HO_2=2OH are also within the most sensitive reactions captured from both the LSA and GSA. This sequence provides an alternative pathway for the formation of OH radicals and competes with the chain-branching reaction R1. A number of C1-C3 reactions are also sensitive both locally and globally: R106: CH_3+H+M=CH_4+M; R127: 2CH_3=C_2H_5+H; R232: C_2H_4+OH=C_2H_3+$_2$O; and R385: C_3H_6=A-C_3H_5+H. On the other hand, larger normalized sensitivity factors are observed for R227: C_2H_4+H(+M)=C_2H_5(+M) and R174: C_2H_2+H(+M)=C_2H_3(+M) based on LSA, whereas according to the GSA, LBV is more sensitive to R199: C_2H_3+O_2=CH_2CHO+O and R175: C_2H_2+O=H+HCCO. Overall, the results of the LSA and GSA indicate that the LBV is largely controlled by the C0-C2 chemistry. None of the reactions involving the fuel or its radicals appear within the top 13 most sensitive reactions. As seen in Fig. 10, the small differences between the total and 1^{st}-order sensitivity indices indicate the weak extend of interaction between the reaction rate constants, i.e., the effects of the input parameters are mainly linear and independent. It is also noted that the sum of the 13 highest 1^{st}-order sensitivity index is around 0.95, as shown in Figure 10, while the sum for all the reactions is above 0.98. These values indicate that higher-order effects do not play a major role for free flame propagation [68].

Figure 11 show the ROP results for H and OH radicals. Considering the impor-

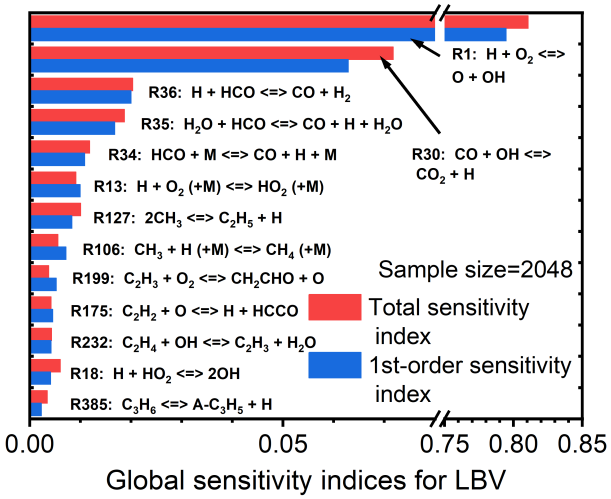

Figure 10: Global sensitivity coefficient on the laminar burning velocity for stoichiometric n-hexane/air mixture under initial conditions of T_0=280 K, P=70 kPa.

tance of active radicals in flame propagation, reactions with significant contribution to the formation of radicals should have significant effect on flame speed. However, although R2: H_2+O<=>H+OH, R4: H_2+OH<=>H+H_2O and R5: 2OH<=>H_2O+O are some of the main contributing reactions for the formations of H and OH radicals, they demonstrate weak sensitivity coefficients and changing their kinetic inputs would not influence the predicted flame speed much. It is also noted that R4 and R5 are also among the main reactions for heat consumption and heat release, respectively.

4.2.2 Analyses under thermal ignition conditions

Normalized local sensitivity coefficients on the ignition delay time and temperature are plotted in Figure 12 with opposite sign since increasing the temperature in the reactor would lead to a decrease of ignition delay time. Figure 13 shows the 1st-order and total global sensitivity indices for IDT. Figure 14 shows the time-resolved ROP for H and OH radicals. The dominance of R5: H+O_2 <=>O+OH in gas autoignition is much lower than under flame propagation conditions. It is also noticed that the sum of higher-order sensitivity indices, i.e., the difference between the total and 1^{st}-order sensitivity indices, for R5 reaches 0.09. This large difference between the global and 1st-order indices indicates that the joint effects of R5 with other reactions are significant. Future study could focus on the combined effects of R5 with other reactions for the optimization of chemical model. As the most important reaction for OH radical formation, R5 accelerates the overall reaction during the induction period and promotes the reactivity of the mixture. Kinetic inputs of another two reactions which are important for OH formation before ignition onset, R90: CH_3+HO_2=CH_3O+OH and R82: CH_3+O_2=CH_2O+OH, also influence the IDT and temperature greatly.

Although there exist differences between the local sensitivity results for ignition

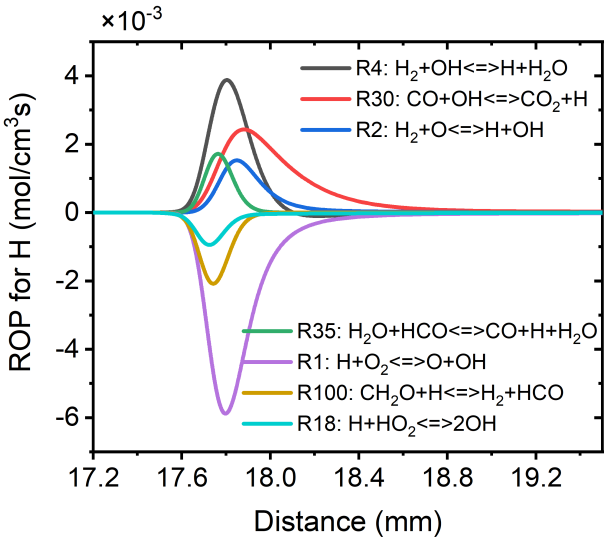

a) H RoP profiles

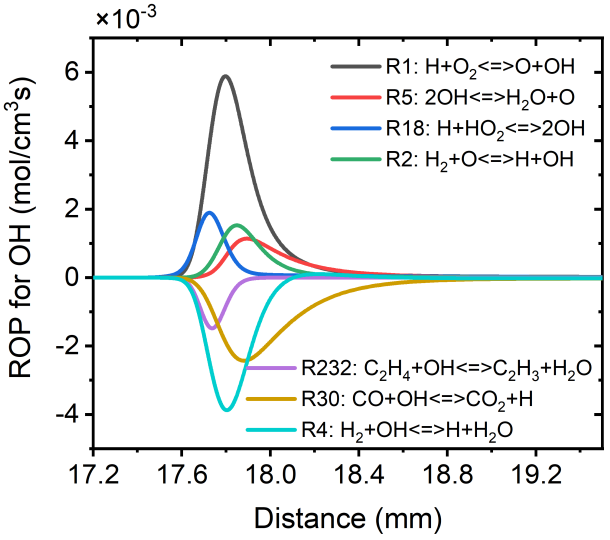

b) OH RoP profiles

Figure 11: Key reactions for the RoP profiles of some active radicals under flame propagation conditions at initial conditions of T_0=280 K, P=70 kPa.

delay time and temperature, identified key reactions with large sensitivity coefficients are very similar. However, when comparing with global sensitivity results, some deviations should be noticed. Based on LSA, IDT is sensitive to the rate constants of R1026: $NC_6H_{14}+OH=C_6H_{13}$-2+H_2O, R135: $CH_2O+OH=H_2O+HCO$ and R31: $2HO_2=H_2O_2+O_2$. From the results of GSA, total sensitivity factors of these three reactions are lower than 0.1%. On the other hand, based on GSA, IDT is sensitive to R137: $CH_2O+CH_3=CH_4+HCO$, R709: $C_4H_7$1-O=$C_2H_4+CH_3CO$ and R1156: $C_2H_4+C_4H_7$1-1=C_6H_{11}3-1, whereas their local sensitivity factors are insignificant. The sum of the 1st-order indices for all the reactions is only 0.853, which indicates significant interactions between the input parameters of the reaction model under auto-ignition conditions.

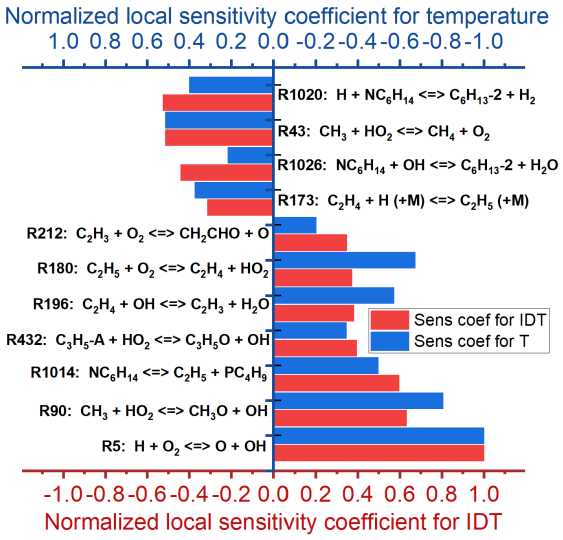

Figure 12: Normalized local sensitivity coefficient on the ignition delay time and temperature for stoichiometric n-hexane/air mixture under initial conditions of T_0=1250 K, P=70 kPa.

It is interesting to note that both the LSA and GSA point out the prominent role of hydrocarbon chemistry under auto-ignition conditions, whereas the reactions of the H-O system do not appear within the most sensitivity ones, with the exception of $H+O_2$=OH+O. From Figure 12 and Figure 13, we can see that the thermal decomposition of n-hexane (R1014) has a larger sensitivity coefficient than H-abstraction reactions by H or OH. From the sensitivity results provided by Zhang et al. [17], the reaction rate of H-abstraction by OH is very important at T=800 K. Due to the lack of sensitivity analysis at high temperature for n-hexane, we compared the present result with the study by Lin et al. [70] who implemented GSA for rich n-decane/air mixture at 1600K and 101 kPa and Lin et al. [58] who performed GSA for stoichiometric n-decane/air mixture at 1000 K and 101 kPa. IDT is sensitive to H-abstraction by HO_2 radical at 1000 K and 101 kPa. At initial conditions of 1600 K and 101 kPa, none of the reactions related to the direct consumption of the n-alkane fuel are important due to the high temperature.

5 Conclusion

Reliable prediction of the combustion properties is important for practical combustion applications, such as evaluating the risk of ignition hazards and flammability in industrial facilities and transportation systems such as aircraft. As a commonly-used aviation kerosene surrogate, n-hexane has been studied through numerical simulations with detailed kinetic mechanisms and experimental measurements for flame properties and shock tube ignition delay times. In the present study, laminar burning velocities were measured for n-hexane/air mixtures at atmospheric and sub-atmospheric pressures using two closed vessels of differing volume. Ignition

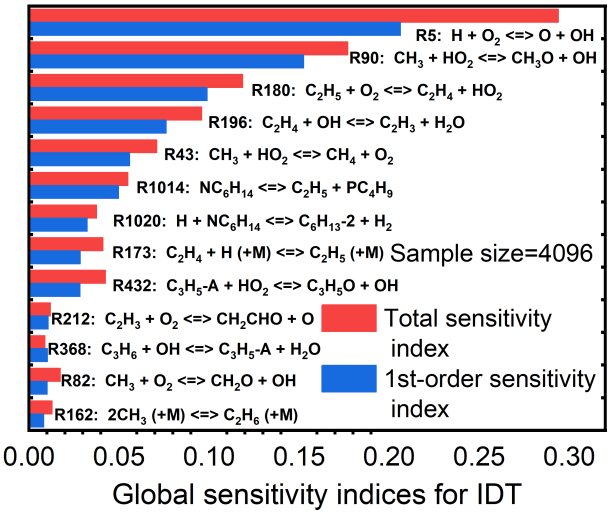

Figure 13: Global sensitivity coefficient on the ignition delay time for stoichiometric n-hexane/air mixture under initial conditions of T_0=1250 K, P=70 kPa.

delay times of stoichiometric n-hexane/O_2/N_2/Ar were measured in a shock tube at temperatures of 1150-1450 K and at pressures of 1.2/2.0 MPa. An experimental database of laminar burning velocity and ignition delay time measured by shock tube was established based on existing literature (LBV data: 111 points in 13 datasets from 6 publications, IDT data: 180 points in 20 datasets from 7 publications) and experimental data from the present study (LBV data: 37 points in 10 datasets, IDT data: 78 points in 4 datasets) for n-hexane-oxygen-diluent mixtures. The capabilities of four chemical models, Curran Mech [17], LLNL Mech [18], JetSurF 2.0 [26] and CaltechMech [30], to reproduce experimental flame properties and ignition delay times were assessed.

For prediction of laminar burning velocity, the overall performance of CaltechMech is better than other three mechanisms, especially at low pressure and low temperature initial conditions. It is also noted that LBV calculated by CaltechMech is larger than that estimated by the other three mechanisms under various conditions. However, the flame speed for lean n-hexane/air mixtures is substantially different than the measured values for all four mechanisms. For predicted ignition delay time, Curran Mech and LLNL Mech show better performances than the two other mechanisms. When the temperature behind the reflected shock wave is higher than 1200 K, LLNL Mech shows better performance than Curran Mech.

Kinetic analyses were implemented to identify important reaction pathways that control the flame propagation and auto-ignition of stoichiometric n-hexane/air mixture at aircraft operation related conditions. Laminar flame speed is sensitive to R1: H+O_2=OH+O and R30: CO+OH=CO_2+H, and to the reactions of HCO with several radicals but not OH. For some reactions which have great effects on active radical formation and heat release rate, their influence on the laminar burning velocity is quite small. Ignition delay time is very sensitive to reactions which would form

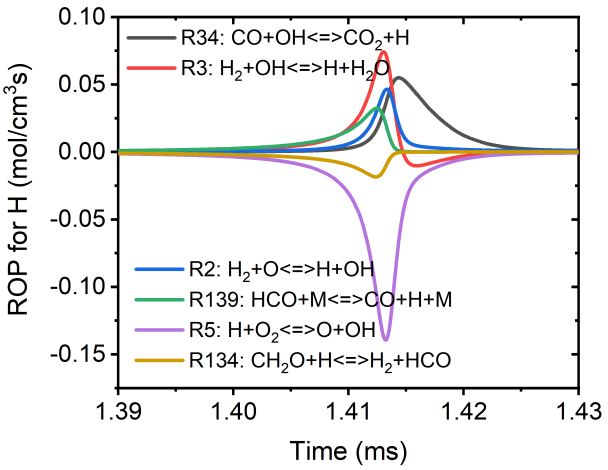

a) H RoP profiles

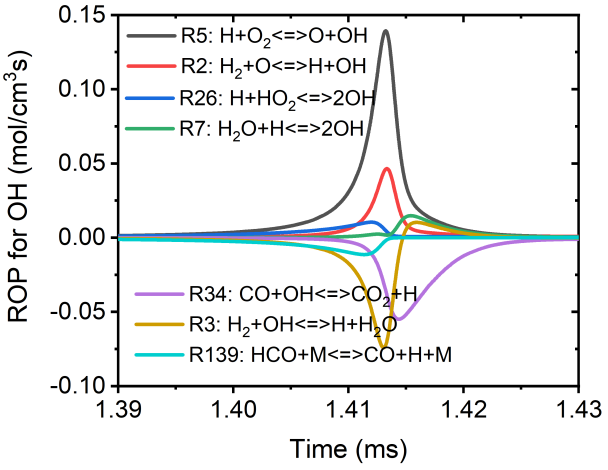

b) OH RoP profiles

Figure 14: Key reactions for the RoP profiles of some active radicals under auto-ignition conditions at initial conditions of T_0=1250 K, P=70 kPa.

OH radical before auto-ignition onset. Thermal decomposition of n-hexane to C_2H_5 and PC_4H_9 shows larger sensitivity coefficient than that of H-abstraction reactions by H, OH, and HO_2 radicals at the target conditions. Deviations may exist between the results from local and global sensitivity analyses. For mechanism optimization in future work, we conclude that both local and global sensitivity analyses should be considered.

6 Acknowledgments

This work was supported in part by The Boeing Company through a Strategic Research and Development Relationship Agreement CT-BA-GTA-1 at the California Institute of Technology. The work performed at ICARE-CNRS Orléans was supported by Centre National de la Recherche Scientifique, CNRS-Ingénierie. NC and AC are grateful to Ilona Cieslak and Agnieszka Jach for their help with the shock

tube experiments.

References

[1] P. Boettcher, R. Mével, V. Thomas, J. Shepherd, The effect of heating rates on low temperature hexane air combustion, Fuel 96 (2012) 392–403.

[2] B. Song, X. Wang, H. Zhang, The aircraft composite integral fuel tank fire safety performance analysis and shrinkage ratio simulation calculation, Procedia Engineering 52 (2013) 320–324.

[3] A. Slippey, K. Bender, C. Tarau, S. Rokkam, Apparatus for characterizing hot surface ignition of aviation fuels, in: 2018 Joint Propulsion Conference.

[4] J. D. Colwell, T. M. Korb, R. E. Peck, Hot surface ignition of Jet-A fuel by conductive deposits, Proceedings of the Combustion Institute 29 (1) (2002) 297–303.

[5] J. D. Colwell, A. Reza, Hot surface ignition of automotive and aviation fluids, Fire Technology 41 (2) (2005) 105–123.

[6] L. R. Boeck, M. Meijers, A. Kink, R. Mével, J. E. Shepherd, Ignition of fuel–air mixtures from a hot circular cylinder, Combustion and Flame 185 (2017) 265–277.

[7] S. Jones, J. Shepherd, Thermal ignition by vertical cylinders, Combustion and Flame 232 (2021) 111499.

[8] C. Martin, J. Shepherd, Low temperature autoignition of Jet A and surrogate jet fuel, Journal of Loss Prevention in the Process Industries 71 (2021) 104454.

[9] S. A. Coronel, J. Melguizo-Gavilanes, R. Mével, J. E. Shepherd, Experimental and numerical study on moving hot particle ignition, Combustion and Flame 192 (2018) 495–506.

[10] A. Dean, O. Penyazkov, K. Sevruk, B. Varatharajan, Autoignition of surrogate fuels at elevated temperatures and pressures, Proceedings of the Combustion Institute 31 (2) (2007) 2481–2488.

[11] Y. He, Y. Wang, C. Grégoire, U. Niedzielska, R. Mével, J. Shepherd, Ignition characteristics of dual-fuel methane-n-hexane-oxygen-diluent mixtures in a rapid compression machine and a shock tube, Fuel 249 (2019) 379–391.

[12] C. Martin, J. Shepherd, Autoignition testing of hydrocarbon fuels using the ASTM-E659 method., Tech. Rep. EDL2020.001, California Institute of Technology (2020).

[13] A. Burcat, E. Olchanski, C. Sokolinski, Kinetics of hexane combustion in a shock tube, Israel Journal of Chemistry 36 (3) (1996) 313–320.

[14] V. Zhukov, V. Sechenov, A. Starikovskii, Ignition delay times in lean n-hexane-air mixture at high pressures, Combustion and Flame 136 (1) (2004) 257–259.

[15] T. Javed, J. Badra, M. Jaasim, E. Es-Sebbar, M. F. Labastida, S. H. Chung, H. G. Im, A. Farooq, Shock tube ignition delay data affected by localized ignition phenomena, Combustion Science and Technology 189 (7) (2017) 1138–1161.

[16] M. Figueroa-Labastida, J. Badra, A. Farooq, Dual-camera high-speed imaging of the ignition modes of ethanol, methanol and n-hexane in a shock tube, Combustion and Flame 224 (2021) 33–42.

[17] K. Zhang, C. Banyon, C. Togbé, P. Dagaut, J. Bugler, H. J. Curran, An experimental and kinetic modeling study of n-hexane oxidation, Combustion and Flame 162 (11) (2015) 4194–4207.

[18] K. Zhang, C. Banyon, U. Burke, G. Kukkadapu, S. W. Wagnon, M. Mehl, H. J. Curran, C. K. Westbrook, W. J. Pitz, An experimental and kinetic modeling study of the oxidation of hexane isomers: Developing consistent reaction rate rules for alkanes, Combustion and Flame 206 (2019) 123–137.

[19] M. Ben Houidi, J. Sotton, M. Bellenoue, Interpretation of auto-ignition delays from RCM in the presence of temperature heterogeneities: Impact on combustion regimes and negative temperature coefficient behavior, Fuel 186 (2016) 476–495.

[20] R. Mével, K. Chatelain, P. Boettcher, G. Dayma, J. Shepherd, Low temperature oxidation of n-hexane in a flow reactor, Fuel 126 (2014) 282–293.

[21] S. G. Davis, C.K. Law, Determination of and fuel structure effects on laminar flame speeds of C_1 to C_8 hydrocarbons, Combustion Science and Technology 140 (1-6) (1998) 427–449.

[22] J. T. Farrell, R. Johnston, I. Androulakis, Molecular structure effects on laminar burning velocities at elevated temperature and pressure, SAE transactions (2004) 1404–1425.

[23] C. Ji, E. Dames, Y. L. Wang, H. Wang, F. N. Egolfopoulos, Propagation and extinction of premixed C_5-C_{12} n-alkane flames, Combustion and Flame 157 (2) (2010) 277–287.

[24] A. Kelley, A. Smallbone, D. Zhu, C. Law, Laminar flame speeds of C_5 to C_8 n-alkanes at elevated pressures: Experimental determination, fuel similarity, and stretch sensitivity, Proceedings of the Combustion Institute 33 (1) (2011) 963–970.

[25] X. Li, E. Hu, X. Lu, S. Huang, Z. Huang, Experimental and kinetic study on laminar flame speeds of hexene isomers and n-hexane, Fuel 243 (2019) 533–540.

[26] H. Wang, E. Dames, B. Sirjean, D. Sheen, R. Tangko, A. Violi, J. Lai, F. Egolfopoulos, D. Davidson, R. Hanson, A high-temperature chemical kinetic model of n-alkane (up to n-dodecane), cyclohexane, and methyl-, ethyl-, n-propyl and n-butyl-cyclohexane oxidation at high temperatures, JetSurF Ver. 2.0, September 19, 2010 (http://web.stanford.edu/group/haiwanglab/JetSurF/JetSurF2.0/index.html).

[27] L. Zhang, H. Ma, Z. Shen, L. Wang, R. Liu, J. Pan, Influence of pressure and temperature on explosion characteristics of n-hexane/air mixtures, Experimental Thermal and Fluid Science 102 (2019) 52–60.

[28] L. Zhang, H. Ma, J. Pan, Z. Shen, L. Wang, R. Liu, K. Zhao, Effects of hydrogen addition on the explosion characteristics of n-hexane/air mixtures, International Journal of Hydrogen Energy 44 (3) (2019) 2029–2038.

[29] K. Yasunaga, H. Yamada, H. Oshita, K. Hattori, Y. Hidaka, H. Curran, Pyrolysis of n-pentane, n-hexane and n-heptane in a single pulse shock tube, Combustion and Flame 185 (2017) 335–345.

[30] G. Blanquart, P. Pepiot-Desjardins, H. Pitsch, Chemical mechanism for high temperature combustion of engine relevant fuels with emphasis on soot precursors, Combustion and Flame 156 (3) (2009) 588–607.

[31] Y. Wu, S. Panigrahy, A. Sahu, C. Bariki, J. Beeckmann, J. Liang, A. Mohamed, S. Dong, C. Tang, H. Pitsch, Z. Huang, H. Curran, Understanding the antagonistic effect of methanol as a component in surrogate fuel models: A case study of methanol/n-heptane mixtures, Combustion and Flame 226 (2021) 229–242.

[32] S. Dong, S. Wagnon, L. Pratali Maffei, G. Kukkadapu, A. Nobili, Q. Mao, M. Pelucchi, L. Cai, K. Zhang, M. Raju, T. Chatterjee, W. Pitz, T. Faravelli, H. Pitsch, P. Senecal, H. Curran, A new detailed kinetic model for surrogate fuels: C3MechV3.3, Applications in Energy and Combustion Science 9 (2022) 100043.

[33] S. Coronel, R. Mevel, S. Bane, J. E. Shepherd, Experimental study of minimum ignition energy of lean H_2-N_2O mixtures, Proceedings of the Combustion Institute 34 (1) (2013) 895–902.

[34] A. Comandini, N. Chaumeix, J. D. Maclean, G. Ciccarelli, Combustion properties of n-heptane/hydrogen mixtures, International Journal of Hydrogen Energy 44 (3) (2019) 2039–2052.

[35] T. Dubois, N. Chaumeix, C.-E. Paillard, Experimental and modeling study of n-propylcyclohexane oxidation under engine-relevant conditions, Energy & Fuels 23 (5) (2009) 2453–2466.

[36] D. Nativel, M. Pelucchi, A. Frassoldati, A. Comandini, A. Cuoci, E. Ranzi, N. Chaumeix, T. Faravelli, Laminar flame speeds of pentanol isomers: An experimental and modeling study, Combustion and Flame 166 (2016) 1–18.

[37] R. Mevel, F. Lafosse, N. Chaumeix, G. Dupre, C.-E. Paillard, Spherical expanding flames in H_2-N_2O-Ar mixtures: Flame speed measurements and kinetic modeling, International Journal of Hydrogen Energy 34 (21) (2009) 9007–9018.

[38] Y. Zhang, S. A. Coronel, R. Mével, Numerical study of synthetic spherically expanding flames for optimization of laminar flame speed experiments, Fuel 310 (2022) 122367.

[39] D. Wang, C. Ji, S. Wang, J. Yang, Z. Wang, Effects of data point number on laminar flame speed extrapolation, Fuel 278 (2020) 118265.

[40] Y. Zhang, M. Jeanson, R. Mével, Z. Chen, N. Chaumeix, Tailored mixture properties for accurate laminar flame speed measurement from spherically expanding flames: Application to $H_2/O_2/N_2$/He mixtures, Combustion and Flame 231 (2021) 111487.

[41] W. Han, P. Dai, X. Gou, Z. Chen, A review of laminar flame speeds of hydrogen and syngas measured from propagating spherical flames, Applications in Energy and Combustion Science 1–4 (2020) 100008.

[42] M. Matalon, B. J. Matkowsky, Flames as gasdynamic discontinuities, Journal of Fluid Mechanics 124 (1982) 239–259.

[43] P. Pelce, P. Clavin, Influence of hydrodynamics and diffusion upon the stability limits of laminar premixed flames, Journal of Fluid Mechanics 124 (1982) 219–237.

[44] G. H. Markstein, Experimental and theoretical studies of flame-front stability, Journal of the Aeronautical Sciences 18 (3) (1951) 199–209.

[45] A. P. Kelley, J. K. Bechtold, C. K. Law, Premixed flame propagation in a confining vessel with weak pressure rise, Journal of Fluid Mechanics 691 (2012) 26–51.

[46] A. P. Kelley, C. K. Law, Nonlinear effects in the extraction of laminar flame speeds from expanding spherical flames, Combustion and Flame 156 (9) (2009) 1844–1851.

[47] C. Olm, I. G. Zsély, R. Pálvölgyi, T. Varga, T. Nagy, H. J. Curran, T. Turányi, Comparison of the performance of several recent hydrogen combustion mechanisms, Combustion and Flame 161 (9) (2014) 2219–2234.

[48] F. N. Egolfopoulos, N. Hansen, Y. Ju, K. Kohse-Hoinghaus, C. K. Law, F. Qi, Advances and challenges in laminar flame experiments and implications for combustion chemistry, Progress in Energy and Combustion Science 43 (2014) 36–67.

[49] Z. Chen, On the accuracy of laminar flame speeds measured from outwardly propagating spherical flames: Methane/air at normal temperature and pressure, Combustion and Flame 162 (6) (2015) 2442–2453.

[50] H.-P. S. Shen, J. Steinberg, J. Vanderover, M. A. Oehlschlaeger, A shock tube study of the ignition of n-heptane, n-decane, n-dodecane, and n-tetradecane at elevated pressures, Energy & Fuels 23 (5) (2009) 2482–2489.

[51] M. Alabbad, Y. Li, K. AlJohani, G. Kenny, K. Hakimov, M. Al-lehaibi, A.-H. Emwas, P. Meier, J. Badra, H. Curran, A. Farooq, Ignition delay time measurements of diesel and gasoline blends, Combustion and Flame 222 (2020) 460–475.

[52] K. P. Chatelain, Y. He, R. Alharbi, R. Mével, E. L. Petersen, D. A. Lacoste, Current status of the high-temperature kinetic models of silane: Part I. Pyrolysis, Combustion and Flame 227 (2021) 526–537.

[53] K. P. Chatelain, Y. He, S. Javoy, R. Mével, E. L. Petersen, D. A. Lacoste, Current status of the high-temperature kinetic models of silane: Part II. Oxidation, Combustion and Flame 227 (2021) 538–549.

[54] D. G. Goodwin, R. L. Speth, H. K. Moffat, B. W. Weber, Cantera: An Object-oriented Software Toolkit for Chemical Kinetics, Thermodynamics, and Transport Processes, 2018.

[55] S. Lapointe, R. A. Whitesides, M. J. McNenly, Sparse, iterative simulation methods for one-dimensional laminar flames, Combustion and Flame 204 (2019) 23–32.

[56] J. J. Scire Jr., F. L. Dryer, R. A. Yetter, Comparison of global and local sensitivity techniques for rate constants determined using complex reaction mechanisms, International Journal of Chemical Kinetics 33 (12) (2001) 784–802.

[57] T. Ziehn, A. S. Tomlin, A global sensitivity study of sulfur chemistry in a premixed methane flame model using HDMR, International Journal of Chemical Kinetics 40 (11) (2008) 742–753.

[58] S. Lin, W. Zhou, Y. Wu, C. K. Law, M. Xie, B. Yang, Evaluation of reduced combustion kinetic mechanisms using global sensitivity-based similarity analysis (GSSA), Proceedings of the Combustion Institute 38 (1) (2021) 1081–1088.

[59] I. M. Sobol, Sensitivity estimates for nonlinear mathematical models., Mathematical Modelling & Computational Experiment 1 (1993) 407–414.

[60] P. Feraboli, M. Miller, Damage resistance and tolerance of carbon/epoxy composite coupons subjected to simulated lightning strike, in: 50th AIAA/ASME/ASCE/AHS/ASC Structures, Structural Dynamics, and Materials Conference, Vol. 40, American Institute of Aeronautics and Astronautics, 2009, pp. 954–967.

[61] Y. Qi, J. Shepherd, Ignition of hexane-air mixtures by highly under-expanded hot jets, Proceedings of the Combustion Institute 39 (3) (2023) :2979–2990.

[62] F. Fisher, J. Plumer, R. Perala, Lightning Protection of Aircraft, Lightning Technologies Incorporated, 2004.

[63] C. Martin, Experiments in thermal ignition: Influence of natural convection on properties of gaseous explosions, Ph.D. thesis, California Institute of Technology (2023).

[64] C. Martin, J. Shepherd, Thermal ignition: Effects of fuel, ambient pressure and nitrogen dilution, Proceedings of the International Symposium on Hazards, Prevention and Mitigation of Industrial Explosions 14.

[65] J. Shepherd, C. Nuyt, J. Lee, Flash point and chemical composition of aviation kerosene (Jet A), Tech. Rep. FM99-4, California Institute of Technology (2000).

[66] R. Mevel, F. Rostand, D. Lemarie, L. Breyton, J. Shepherd, Oxidation of n-hexane in the vicinity of the auto-ignition temperature, Fuel 236 (2019) 373–381.

[67] D. A. Sheen, H. Wang, The method of uncertainty quantification and minimization using polynomial chaos expansions, Combustion and Flame 158 (12) (2011) 2358–2374.

[68] J. Zador, I. G. Zsely, T. Turanyi, M. Ratto, S. Tarantola, A. Saltelli, Local and global uncertainty analyses of a methane flame model, The Journal of Physical Chemistry A 109 (43) (2005) 9795–9807.

[69] H. Wang, D. A. Sheen, Combustion kinetic model uncertainty quantification, propagation and minimization, Progress in Energy and Combustion Science 47 (2015) 1–31.

[70] K. Lin, Z. Zhou, C. K. Law, B. Yang, Dimensionality reduction for surrogate model construction for global sensitivity analysis: Comparison between active subspace and local sensitivity analysis, Combustion and Flame 232 (2021) 111501.

A comprehensive experimental and kinetic modeling study of flame speed and ignition delay time in n-hexane-based mixtures

Yakun Zhang[a], Stephanie A. Coronel[b], Simon Lapointe[b], Vaughan L. Thomas[c], Rémy Mével[d,*], Andrea Comandini[e], Nabiha Chaumeix[e], Joseph E. Shepherd[b]

[a]*School of Vehicle and Mobility, Tsinghua University, Beijing, China*
[b]*Graduate Aerospace Laboratories, California Institute of Technology, Pasadena, California 91125, USA*
[c]*Department of Mechanical Engineering, Johns Hopkins University, Baltimore, Maryland 21218,USA*
[d]*School of Aeronautics and Astronautics, Zhejiang University, Hangzhou, China*
[e]*ICARE, CNRS-INSIS, 1C Avenue de la Recherche Scientifique, 45071 Orléans Cedex 2, France*

1. Extrapolation surface

Example extrapolation surfaces for laminar flame speed S_u^0 and Markstein length L_b are shown in Fig. 1. In Fig. 1 a), an obvious folding which is induced by ignition effect exists. In Fig. 1 b), significant effect of flame instability caused the crests. In Fig. 1 c), the surfaces are wavy with small oscillations. It should be noted that the peak in Fig. 1 c) is induced by small radius range for extrapolation.

Fig. 2 shows corresponding extrapolation curves obtained with several equations. In Fig. 2 (a), the four equations provide similar results. In Fig. 2 (b), the three non-linear equations provide similar results, whereas the linear equation leads to a significantly larger flame speed, which is not taken into account to determine the average flame speed.

*Corresponding author: mevel@zju.edu.cn

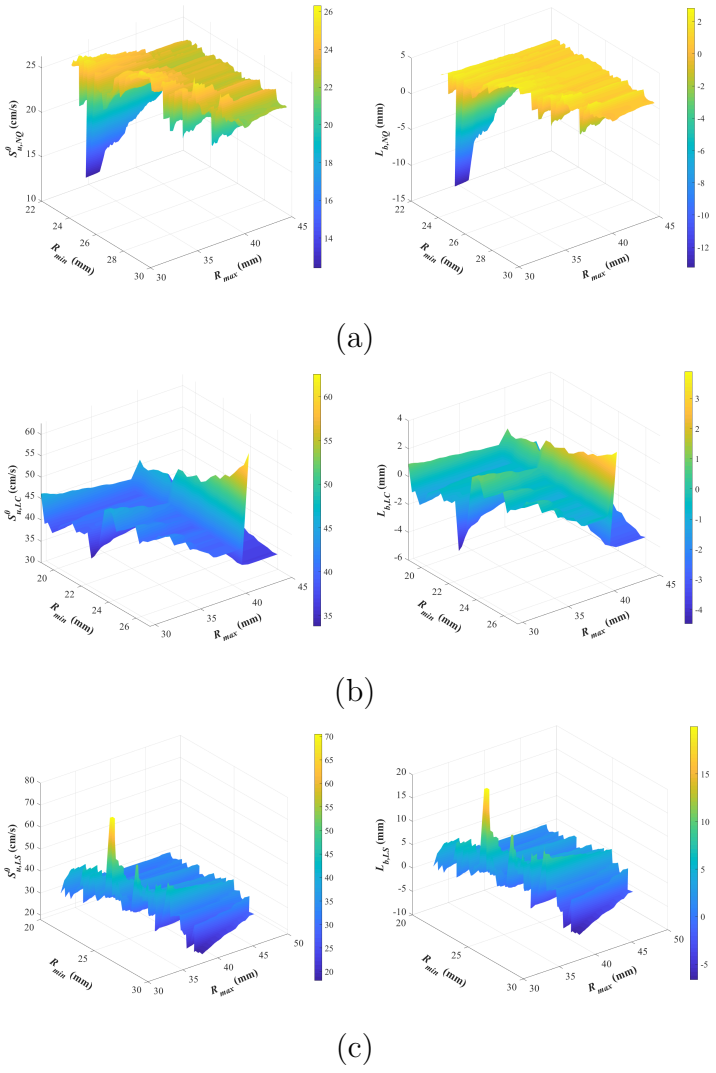

Fig. 1. Example extrapolation surfaces for laminar flame speed S_u^0 and Markstein length L_b under various flame radius range for n-hexane/air mixtures. Conditions: (a)P_{in}=100 kPa, T_{in}=295 K, Φ=0.764; (b)P_{in}=50 kPa, T_{in}=295 K, Φ=1.303; (c)P_{in}=50 kPa, T_{in}=295 K, Φ=0.9;.

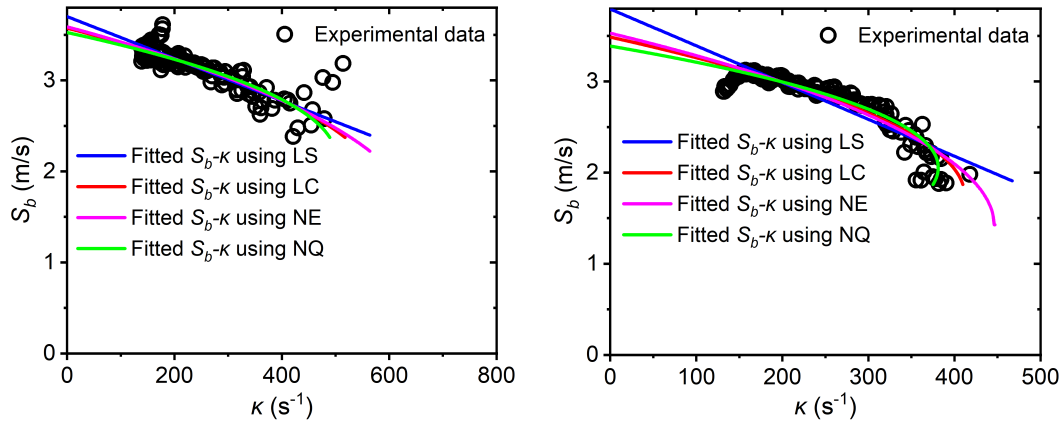

Fig. 2. Example extrapolation curves for laminar flame speed S_u^0 for n-hexane/air mixtures. Conditions: (a)P_{in}=50 kPa, T_{in}=295 K, Φ=1.1; (b) P_{in}=50 kPa, T_{in}=295 K, Φ=1.0.

2. Experimental data

The experimental ignition delay time and laminar burning velocity data from the present study is provided here.

Number	P (kPa)	T (K)	Φ	S_u^0 (cm/s)	$\delta_{S_u^0}$ (cm/s)	L_b (mm)	δ_{L_b} (mm)
1	100	295	0.764	22.860	0.377	1.156	0.256
2	100	295	0.829	30.073	1.305	1.633	0.800
3	100	295	0.900	33.067	0.500	0.735	0.162
4	100	295	0.980	36.710	0.945	1.261	0.460
5	100	295	1.260	37.379	0.213	-0.026	0.031
6	100	295	1.433	28.451	1.244	-1.055	0.540
7	50	295	0.857	34.496	0.223	0.928	0.800
8	50	295	0.900	35.681	0.713	1.453	0.394
9	50	295	0.952	40.276	1.204	1.785	0.692
10	50	295	1.000	41.228	3.257	1.782	1.035
11	50	295	1.103	43.878	1.357	1.860	0.370
12	50	295	1.198	41.712	0.600	0.933	0.240
13	50	295	1.303	38.175	0.487	-0.139	0.183

14	50	295	1.341	34.378	0.189	0.329	0.031
15	50	295	1.399	29.031	1.178	-2.118	0.899
16	50	295	1.438	25.664	0.207	-2.589	0.376
17	50	295	1.495	19.868	0.627	-3.868	0.442
18	50	295	1.602	14.118	0.433	-5.290	0.405
19	50	313	0.904	38.542	0.362	0.194	0.194
20	50	312.4	1.103	45.997	1.746	1.463	0.648
21	50	312.9	1.409	32.187	0.261	-0.207	0.283
22	50	325.7	0.904	42.723	0.288	1.881	0.648
23	50	325.4	1.103	53.311	0.345	2.382	1.008
24	50	325.3	1.399	35.548	0.323	-0.149	0.120
25	50	332.7	0.895	41.124	0.765	1.206	0.379
26	50	357.4	0.904	50.872	1.333	1.671	0.600
27	50	357.5	1.103	58.771	2.522	1.842	0.882
28*	50	380.2	0.904	57.832	0.535	2.373	0.778
29*	50	380.3	1.103	63.693	1.938	1.550	0.621
30*	50	380.1	1.399	45.623	0.307	-0.077	0.225
31	50	357.6	1.399	40.218	0.228	-0.090	0.172
32	100	356.7	0.900	45.841	0.908	1.315	0.424
33	80	356.8	0.900	45.373	0.930	1.035	0.342
34	40	356.5	0.900	50.404	0.527	1.787	0.245

Table 1: Experimental laminar burning velocities and Markstein lengths for n-hexane/air mixtures.

*: experiments were performed at ICARE-CNRS Orléans.

Number	X_{NC6H14}	X_{O2}	X_{N2}	X_{Ar}	Φ	P_5 (MPa)	T_5 (K)	dP_5/dt (%/ms)	τ_P (μs)	$\tau_{50\%OH}$ (μs)
1	0.0024	0.0228	0.0859	0.8889	1.0	1.330	1448.54	27.23		100.6
2	0.0024	0.0227	0.0854	0.8895	1.0	1.387	1425.53	5.00		140.0
3	0.0024	0.0228	0.0859	0.8889	1.0	1.368	1414.26	8.42		151.2
4	0.0024	0.0227	0.0854	0.8895	1.0	1.332	1385.43	23.66		231.8
5	0.0024	0.0228	0.0858	0.8889	1.0	1.309	1362.13	20.19		294.8
6	0.0021	0.0206	0.0774	0.8999	0.97	1.306	1320.62	3.88	531.92	500.8
7	0.0024	0.0228	0.0858	0.8889	1.0	1.286	1319.83	7.07	515.1	483.2
8	0.0021	0.0206	0.0774	0.8999	0.97	1.269	1300.50	7.04	674.83	
9	0.0024	0.0228	0.0859	0.8889	1.0	1.209	1294.30	10.70	643.1	625.7
10	0.0024	0.0228	0.0859	0.8889	1.0	1.221	1284.53	13.09	687.4	679.0
11	0.0024	0.0228	0.0859	0.8889	1.0	1.239	1272.31	7.81	801.7	823.7
12	0.0024	0.0228	0.0859	0.8889	1.0	1.247	1272.30	5.47	866.14	902.71
13	0.0024	0.0228	0.0858	0.8889	1.0	1.226	1270.54	7.72	769.26	793.69
14	0.0024	0.0228	0.0859	0.8889	1.0	1.312	1260.89	4.77	886.46	915.48
15	0.0024	0.0228	0.0859	0.8889	1.0	1.247	1247.43	6.76	957.12	1007.69
16	0.0024	0.0227	0.0854	0.8895	1.0	1.202	1223.67	11.61	1255.7	1410.3
17	0.0024	0.0228	0.0858	0.8889	1.0	1.094	1213.39	9.70	1038.9	1189.2
18	0.0024	0.0228	0.0859	0.8889	1.0	1.180	1212.09	7.15	1557.68	1705.91

19	0.0024	0.0228	0.0858	0.8889	1.0	1.107	1208.91	8.57	1451.32	
20	0.00216	0.02055	0.07726	0.90003	1.0	2.261	1434.46	37.81	111.83	109.92
21	0.00216	0.02054	0.07724	0.90006	1.0	2.144	1385.65	8.67	180.7	203.3
22	0.00216	0.02054	0.07725	0.90005	1.0	1.958	1365.91	30.90	302.64	245.53
23	0.00216	0.02054	0.07725	0.90005	1.0	2.081	1363.40	30.05	287.4	251.15
24	0.00216	0.02055	0.07726	0.90003	1.0	1.841	1363.38	23.20	295.1	269.9
25	0.00216	0.02055	0.07726	0.90003	1.0	2.030	1337.72	31.90	356.55	333.44
26	0.00216	0.02055	0.07726	0.90003	1.0	1.973	1332.49	19.27	383.24	352.91
27	0.00216	0.02054	0.07722	0.90008	1.0	2.007	1321.97	13.53	459.9	420.59
28	0.00216	0.02055	0.07726	0.90004	1.0	2.069	1321.54	21.37	407.75	442.74
29	0.00216	0.02054	0.07724	0.90006	1.0	1.951	1291.21	27.29	571.86	577.43
30	0.00215	0.02053	0.07720	0.90011	1.0	1.882	1289.85	10.00		618.45
31	0.00216	0.02054	0.07724	0.90006	1.0	2.019	1287.02	18.32	694.08	675.61
32	0.00216	0.02054	0.07724	0.90006	1.0	1.984	1271.21	21.42	679.4	706.9
33	0.00216	0.02055	0.07726	0.90004	1.0	1.911	1269.01	26.01	641.98	703.86
34	0.00215	0.02053	0.07720	0.90011	1.0	1.804	1265.60	20.58	761.41	815.95
35	0.00215	0.02053	0.07720	0.90011	1.0	1.827	1265.33	17.82	776.69	759.14
36	0.00216	0.02054	0.07722	0.90008	1.0	1.803	1263.21	17.40	816.54	829.03
37	0.00216	0.02055	0.07726	0.90004	1.0	1.852	1246.27	24.77	862.33	922.28

38	0.00216	0.02054	0.07723	0.90006	1.0	1.891	1220.35	16.71	1106.9	1249.3
39	0.00216	0.02054	0.07724	0.90006	1.0	1.786	1209.77	17.46	1332.09	1411.61
40	0.00216	0.02054	0.07723	0.90006	1.0	1.949	1202.31	16.63	1377.44	1484.16
41	0.00216	0.02054	0.07724	0.90006	1.0	1.893	1202.02	13.71	1479.22	1530.58
42	0.00216	0.02054	0.07722	0.90008	1.0	1.758	1160.81	13.94	1826.05	2051.67

Table 2: Experimental ignition delay times for n-hexane/O_2/N_2/Ar mixtures.

3. Error values for mechanism evaluation

				Error			
Reference	P (kPa)	T (K)	Pts	Caltech	Jetsurf	Curran	LLNL
Present study	100	295	6	24.82	181.40	143.40	136.08
	50	295	12	31.79	94.71	111.66	124.49
	50	313	3	91.93	168.40	217.39	234.72
	50	325	3	82.06	200.31	184.58	190.25
	50	332	1	84.99	35.55	39.08	49.19
	50	357	3	30.25	167.18	183.12	188.02
	50	380	3	16.88	144.80	140.55	143.77
	100	357	1	4.82	1.28	0.77	0.05
	80	357	1	24.23	2.94	4.56	7.80
	40	357	1	111.25	28.76	54.74	65.58
Total			**37**	**41.74**	**127.52**	**131.67**	**138.33**

Table 3: Evaluation of the predictions of CaltechMech, Jetsurf 2, Curran Mech and LLNL Mech for LBV in n-hexane/air mixtures based on the LBV data from present study.

				Error			
Reference	P (kPa)	T (K)	Pts	Caltech	Jetsurf	Curran	LLNL
Davis et al. 1998 [1]	101	298	13	0.55	2.51	2.16	2.00
Farrel et al. 2004 [2]	304	450	9	23.69	60.81	56.44	52.21
Ji et al. 2004 [3]	101	353	10	10.19	6.41	6.06	4.41
Kelley et al. 2011 [4]	101	353	19	5.01	1.24	1.87	2.16
	203	353	7	2.89	0.84	0.55	0.44
	507	353	5	1.01	0.49	0.79	0.44
	1013	353	3	0.60	0.19	0.45	0.25
Li et al. 2019 [5]	100	373	8	5.58	1.24	1.55	1.90
Zhang et al. 2019 [6]	60	353	9	8.48	8.36	7.11	6.02
	80	353	9	17.19	6.74	6.12	5.64
	100	353	9	58.06	27.75	29.04	29.48
	100	373	9	57.53	32.23	33.22	32.56
	100	393	9	70.76	42.24	43.75	42.89
Total			**111**	**20.27**	**14.64**	**14.73**	**14.08**

Table 4: Evaluation of the predictions of CaltechMech, Jetsurf 2, Curran Mech and LLNL Mech for LBV in n-hexane/air mixtures based on the LBV data from published literature.

			Dilution				Error			
P (MPa)	T (K)	Φ	Ar/N2	%	Method	Pts	Caltech	Jetsurf	Curran	LLNL
1.094-1.387	1209-1449	1.0	N2+Ar	88.89	$(dP/dt)_{max}$	14	3.03	3.03	2.70	**0.95**
					50% OH^*_{max}	19	2.62	2.85	2.37	**1.40**
1.781-2.291	1161-1434	1.0	N2+Ar	90.0	$(dP/dt)_{max}$	22	4.05	3.31	**2.48**	7.81
					50% OH^*_{max}	23	2.05	1.21	**0.96**	4.62

Table 5: Evaluation of the predictions of CaltechMech, Jetsurf 2, Curran Mech and LLNL Mech for IDT in n-hexane/O_2/N_2/Ar mixtures based on the IDT data from present study.

				Dilution				Error			
Reference	P (MPa)	T (K)	Φ	Ar/N2	%	Method	Pts	Caltech	Jetsurf	Curran	LLNL
Burcat et al.	0.36-0.43	1360-1520	1.0	Ar	89.5	$(dP/dt)_{max}$	3	2.05	1.58	1.0	1.99
1996 [7]	0.38-0.40	1200-1430	0.5	Ar	79.8	$(dP/dt)_{max}$	3	14.26	8.71	6.71	6.44
	0.34-0.38	1360-1760	2.0	Ar	94.2	$(dP/dt)_{max}$	3	10.20	14.66	8.06	10.34
	0.36-0.37	1280-1570	0.5	Ar	90.0	$(dP/dt)_{max}$	3	13.94	19.54	14.38	19.51
	0.30-0.32	1320-1460	1.0	Ar	79.0	$(dP/dt)_{max}$	3	8.62	6.45	2.90	3.19
	0.35-0.36	1260-1460	2.0	Ar	88.5	$(dP/dt)_{max}$	3	12.86	13.60	8.36	8.34
	0.76-0.84	1360-1480	1.0	Ar	94.8	$(dP/dt)_{max}$	3	7.49	6.70	5.48	9.95
Zhukov et al.	1.15-1.40	1170-1380	0.5	N2	78.1	OH^*_{max}	13	12.41	6.03	4.11	3.86
2004 [8]	5.57-6.69	1030-1350	0.5	N2	78.1	OH^*_{max}	16	5.04	2.72	3.62	1.52
	20.87-24.72	820-1190	0.5	N2	78.1	OH^*_{max}	11	9.9	188.65	10.41	15.29
Figueroa-Labastida et al.	0.23-0.24	1080-1370	1.0	Ar	89.5	$(dP/dt)_{max}$	4	43.62	31.58	27.61	25.98
2021 [9]	0.24-0.27	820-990	1.0	Ar	47.5	$(dP/dt)_{max}$	3	190.14	397.18	166.52	155.27
He et al.	0.32-0.38	1300-1479	0.66	Ar	96.0	OH^*_{max}	9	4.97	3.58	3.06	2.59
2019 [10]	0.31-0.41	1300-1580	1.0	Ar	96.0	OH^*_{max}	11	4.63	4.61	3.99	2.66
	0.31-0.37	1340-1610	2.0	Ar	96.0	OH^*_{max}	18	3.73	5.73	6.40	4.77
Javed et al.	0.15	640-1260	1.1	Ar	51.0	OH^*_{max}	13	79.43	86.20	51.01	51.01
2017 [11]											

Zhang et al.	1.52	740-1360	1.0	N2	77.30	$(dP/dt)_{max}$	15	13.15	65.95	2.87	3.57
2015 [12]	1.52	750-1320	2.0	N2	75.70	$(dP/dt)_{max}$	17	15.95	112.28	5.49	6.71
	3.24	800-1350	1.0	N2	77.30	$(dP/dt)_{max}$	14	12.98	167.86	4.46	6.46
Zhang et al.	1.50	740-1360	1.0	N2	77.30	$(dP/dt)_{max}$	15	15.50	105.04	2.80	3.76
2019 [13]											
Total							**180**	**18.79**	**65.88**	**11.48**	**11.68**

Table 6: Evaluation of the predictions of CaltechMech, Jetsurf 2, Curran Mech and LLNL Mech for IDT in n-hexane-based mixtures based on the IDT data from published literature.

4. Performance of reduced mechanisms

Predictions of reduced CaltechMech were compared with those of CaltechMech, shown in Fig. 3. It turns out the flame propagation processes predicted by initial CaltechMech and reduced CaltechMech are pretty similar under various initial thermodynamic conditions.

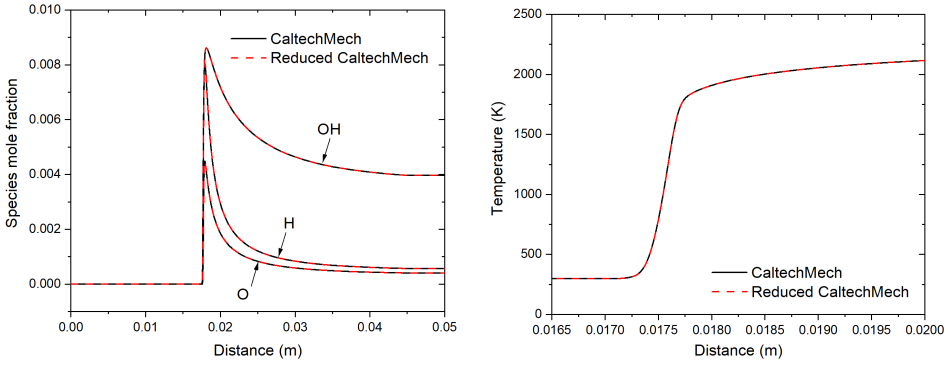

(a) P=1 atm, T_0=298 K, Φ=1.0

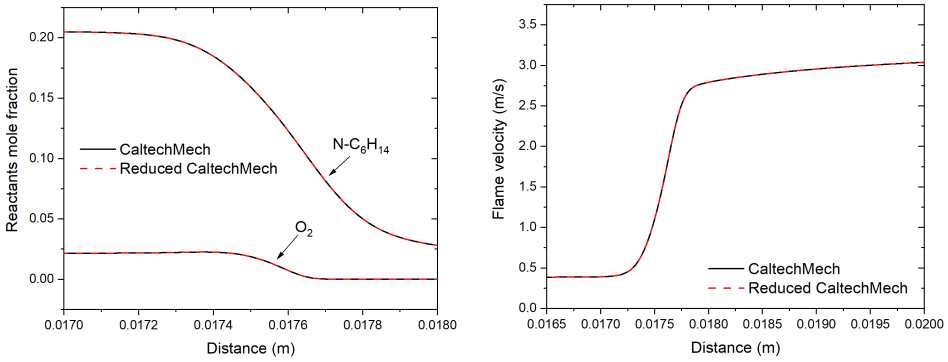

(b) P=70 kPa, T_0=280 K, Φ=1.0

Fig. 3. Comparisons of species, thermodynamic parameter and velocity profiles between reduced and initial CaltechMech.

The performance of the reduced LLNL Mech was evaluated through comparing with the predictions of detailed LLNL Mech, shown in Fig. 4. Calculated ignition delay times were compared in Table 7. It is seen that reduced LLNL Mech predicts slower n-hexane consumption which leads to larger estimation for auto-ignition onset.

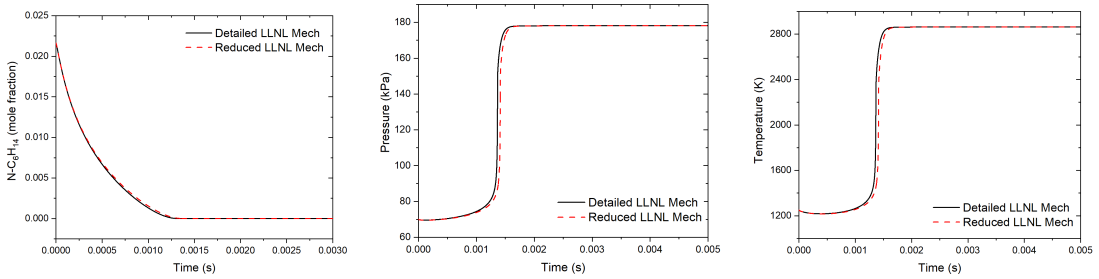

Fig. 4. Comparisons of species and thermodynamic parameter profiles between reduced and initial LLNL Mech. Condition: P=70 kPa, T_0=280 K, Φ=1.0.

	IDT (ms)		Relative
Condition	Detailed Mech	Reduced Mech	error
T=1250 K, P=70 kPa, Φ=1.0	1.365	1.413	3.50%
T=1200 K, P=70 kPa, Φ=1.0	2.693	2.819	4.71%
T=1300 K, P=70 kPa, Φ=1.0	0.721	0.740	2.60%
T=1250 K, P=69 kPa, Φ=1.0	1.378	1.426	3.48%
T=1250 K, P=71 kPa, Φ=1.0	1.352	1.399	3.52%
T=1250 K, P=70 kPa, Φ=0.9	1.295	1.337	3.20%
T=1250 K, P=70 kPa, Φ=1.1	1.432	1.486	3.78%

Table 7: Comparisons of predicted IDTs between reduced and initial LLNL Mech.

5. Global sensitivity results with different sample sizes

The convergence of the global sensitivity indices under different sample sizes was tested in order to obtain accurate result. For global sensitivity analysis using reduced CaltechMech, calculated indices for laminar flame speed are presented in Table 8.

		Sample size N			
Reaction	Index type	N=256	N=512	N=1024	N=2048
R1:	1st-order	0.737209	0.737763	0.799752	0.794699
$H+O_2$ <=>O+OH	total	0.832713	0.809960	0.802813	0.810666
R13:	1st-order	0.016118	0.014390	0.010467	0.009968

$H+O_2(+M)<=>HO_2(+M)$	total	0.009129	0.009053	0.009098	0.009121
R20:	1st-order	0.000663	0.001176	0.001327	0.001433
$HO_2+OH<=>H_2O+O_2$	total	0.002196	0.002047	0.002039	0.002022
R170:	1st-order	0.000784	0.000444	0.001431	0.001427
HCCO+OH=>CO+H+HCO	total	0.001543	0.001509	0.001508	0.001503
R175:	1st-order	0.012408	0.008733	0.004443	0.004547
$C_2H_2+O<=>H+HCCO$	total	0.004332	0.004360	0.004309	0.004234

Table 8: 1st-order and total global sensitivity indices for laminar flame speed with different sample sizes using reduced CaltechMech.

For global sensitivity analysis using reduced LLNL Mech, calculated indices for ignition delay time are presented in Table 9.

		Sample size N			
Reaction	Index type	N=512	N=1024	N=2048	N=4096
R27:	1st-order	0.004623	0.003392	0.003012	0.003546
$H+HO_2 <=>H_2+O_2$	total	0.004196	0.004336	0.004329	0.004292
R43:	1st-order	0.056529	0.052922	0.054177	0.055985
$CH_3+HO_2 <=>CH_4+O_2$	total	0.079055	0.074764	0.071364	0.071137
R82:	1st-order	0.012288	0.008348	0.010791	0.010228
$CH_3+O_2 <=>CH_2O+OH$	total	0.017977	0.017728	0.017175	0.017499
R356:	1st-order	0.015639	0.003770	0.004707	0.004667
$C_3H_6 <=>C_3H_5$-A+H	total	0.004623	0.005087	0.005234	0.005054
R432:	1st-order	0.025310	0.027342	0.028449	0.028472
C_3H_5-A+$HO_2 <=>C_3H_5O+OH$	total	0.039563	0.042953	0.044173	0.042580

Table 9: 1st-order and total global sensitivity indices for ignition delay time with different sample sizes using reduced LLNL Mech.

References

[1] S. G. Davis, C.K. Law, Determination of and fuel structure effects on laminar flame speeds of C_1 to C_8 hydrocarbons, Combustion Science and Technology 140 (1-6) (1998) 427–449.

[2] J. T. Farrell, R. Johnston, I. Androulakis, Molecular structure effects on laminar burning velocities at elevated temperature and pressure, SAE transactions (2004) 1404–1425.

[3] C. Ji, E. Dames, Y. L. Wang, H. Wang, F. N. Egolfopoulos, Propagation and extinction of premixed C_5-C_{12} n-alkane flames, Combustion and Flame 157 (2) (2010) 277–287.

[4] A. Kelley, A. Smallbone, D. Zhu, C. Law, Laminar flame speeds of C_5 to C_8 n-alkanes at elevated pressures: Experimental determination, fuel similarity, and stretch sensitivity, Proceedings of the Combustion Institute 33 (1) (2011) 963–970.

[5] X. Li, E. Hu, X. Lu, S. Huang, Z. Huang, Experimental and kinetic study on laminar flame speeds of hexene isomers and n-hexane, Fuel 243 (2019) 533–540.

[6] L. Zhang, H. Ma, Z. Shen, L. Wang, R. Liu, J. Pan, Influence of pressure and temperature on explosion characteristics of n-hexane/air mixtures, Experimental Thermal and Fluid Science 102 (2019) 52–60.

[7] A. Burcat, E. Olchanski, C. Sokolinski, Kinetics of hexane combustion in a shock tube, Israel Journal of Chemistry 36 (3) (1996) 313–320.

[8] V. Zhukov, V. Sechenov, A. Starikovskii, Ignition delay times in lean n-hexane-air mixture at high pressures, Combustion and Flame 136 (1) (2004) 257–259.

[9] M. Figueroa-Labastida, J. Badra, A. Farooq, Dual-camera high-speed imaging of the ignition modes of ethanol, methanol and n-hexane in a shock tube, Combustion and Flame 224 (2021) 33–42.

[10] Y. He, Y. Wang, C. Grégoire, U. Niedzielska, R. Mével, J. E. Shepherd, Ignition characteristics of dual-fuel methane-n-hexane-oxygen-diluent mixtures in a rapid compression machine and a shock tube, Fuel 249 (2019) 379–391.

[11] T. Javed, J. Badra, M. Jaasim, E. Es-Sebbar, M. F. Labastida, S. H. Chung, H. G. Im, A. Farooq, Shock tube ignition delay data affected by localized ignition phenomena, Combustion Science and Technology 189 (7) (2017) 1138–1161.

[12] K. Zhang, C. Banyon, C. Togbé, P. Dagaut, J. Bugler, H. J. Curran, An experimental and kinetic modeling study of n-hexane oxidation, Combustion and Flame 162 (11) (2015) 4194–4207.

[13] K. Zhang, C. Banyon, U. Burke, G. Kukkadapu, S. W. Wagnon, M. Mehl, H. J. Curran, C. K. Westbrook, W. J. Pitz, An experimental and kinetic modeling study of the oxidation of hexane isomers: Developing consistent reaction rate rules for alkanes, Combustion and Flame 206 (2019) 123–137.